DEVELOPMENT OF A LIGHTWEIGHT LAMINATED COMPOSITE WHEEL FOR FORMULA SAE RACE VEHICLES

By

Hans Walther

Submitted to the graduate degree program in Mechanical Engineering and the Graduate Faculty of the University of Kansas in partial fulfillment of the requirements for the degree of Master of Science.

_____

Chairperson: Dr. Robert M. Sorem

_____

Dr. Mark Ewing

_____

Dr. Richard Hale

Date Defended: June 07, 2016

The Thesis Committee for Hans Walther

certifies that this is the approved version of the following thesis:

DEVELOPMENT OF A LIGHTWEIGHT LAMINATED COMPOSITE WHEEL FOR FORMULA SAE RACE VEHICLES

_____

Chairperson: Dr. Robert M. Sorem

Date approved: June 07, 2016

Abstract

Reducing the weight of a racing vehicle can substantially improve its acceleration and general performance abilities. More specifically, reduction of the unsprung corner weight can provide noticeable performance gains in handling and responsiveness, leading to a quicker, more agile car due to a lower yawing moment of inertia. Unsprung weight reduction also improves the car's ability to maintain contact between the tires and the road surface for more consistent grip. The unsprung mass is mostly made up of the tires, wheels, and other components housed within the wheel package. The effect of this weight is especially significant in open-wheeled racecars because this mass is the furthest from the car's center of gravity. This is exactly the case for the Formula SAE (FSAE) race vehicles considered in this thesis.

Decreasing the weight of the wheel itself is a straightforward approach to reducing the unsprung corner weight as well as rotating mass. Even though there are various commercially available wheels for FSAE cars, the lightest aluminum options have plateaued in weight minimization. Also, maintaining high stiffness is important to minimize compliance and maintain favorable suspension dynamics, specifically camber. So, the idea of a lighter composite wheel is proposed. With the goal of developing a lightweight and stiff wheel, composite materials such as carbon fiber reinforced plastics are a good alternative to conventional metals due to their high stiffness to weight ratios. Through the use of finite element analysis software and physical testing, a laminated composite wheel was developed for the Jayhawk Motorsports FSAE racecars. The composite wheel is significantly lighter than the aluminum benchmark and maintains structural integrity as designed for the load cases compared herein. The details of its development are presented throughout the text of this thesis.

Acknowledgements

The work of this master's thesis project was carried out in collaboration with the Jayhawk Motorsports Formula SAE team at the University of Kansas, and I am grateful to have had that opportunity. I thank the team for their assistance and all the resources they shared, especially Philip Twist and Taylor Lawson for their help with the CNC machining processes and Alec Rounds for his technical support. Sincere thanks to my advisor, Dr. Robert Sorem, for his guidance, advice and support throughout my undergraduate and graduate studies. I would also like to thank my committee members, Dr. Richard Hale and Dr. Mark Ewing for their time and expertise. The support of those mentioned is greatly appreciated.

Table of Contents

List of Tables

List of Figures

Abbreviations

CAD	Computer aided drafting
CFRP	Carbon fiber reinforced plastic
E	Elastic or Young's modulus
F	Material strength
FEA	Finite element analysis
FRP	Fiber reinforced plastic
FSAE	Formula SAE
JMS	Jayhawk Motorsports
LC	Load case
PW	Plain weave
FS	Safety Factor
RF	Reserve factor
SAE	Society of Automotive Engineers
TTC	Tire Test Consortium
TRA	Tire and Rim Association
Uni	Unidirectional tape
v	Poisson's ratio

Notes:

Rim and wheel are used synonymously throughout the thesis, as are safety factor and reserve factor.

1 Introduction

Automotive racing is an exciting and extremely competitive sport that is popular internationally with hundreds of different series for amateur and professional racers of all levels. The significance and presence of improved vehicle design, engineering and development has greatly increased over the years thanks to advancements in engineering and manufacturing technologies in racing. Each race vehicle's ability to compete and perform is dependent on many different design factors, but perhaps one of the most common efforts made by designers is to decrease the vehicle's weight wherever possible. Because race cars are made up of so many different components, weight reduction is possible in various ways, but one area that many agree to have significant effect on performance and handling is the reduction of unsprung corner mass.

Unique design and development opportunities are especially possible within racing series that allow for more freedom in overall vehicle design. A great example of this is the Formula SAE (FSAE) international collegiate competition series. In FSAE, engineering students design and build open-wheeled, single-seat race car prototypes per the rules and guidelines of the Formula SAE rulebook [1]. These students then compete with and race their vehicles at competitions all over the world with the purpose of displaying and proving their unique designs and automotive engineering abilities.

This thesis investigates the development of a lightweight 13 inch composite wheel for FSAE racing, designed specifically for the Jayhawk Motorsports (JMS) race cars.

Figure 1.1: 2013 JMS race car

1.1 Objectives

The focus of this thesis to is to provide a detailed account of the development process for an improved, lightweight composite rim to be used on the JMS race cars. Such a wheel could also be utilized by other FSAE teams as well as various lightweight race cars such as those in SCCA formula classes. It is most common for FSAE teams to purchase commercially available metallic rims, as opposed to designing and manufacturing their own. This is an easy choice mainly for time and simplicity's sake, and because these purchased parts have been proven to work as they usually come from well-established wheel manufacturers. However, a number of teams have made efforts to successfully produce their own rims that are lighter than the commercially available options, some of which use composite materials. JMS is one of those teams, but it is suspected that further improvements can be made to

current and previous designs. As is common with most structural components, computer aided drafting (CAD) and finite element analysis (FEA) software packages are used for design and analysis. However, common limitations to computational resources, funding and high-end testing equipment often leads to oversimplified simulations with a lack of result validation options. For this thesis, a comprehensive and adjustable FEA model has been developed for the composite rim design, and simple low-cost benchmarking simulations and physical tests are explored as validation methods. In addition, the issue of limited resources for the manufacturing of composite structures was also explored.

1.2 Delimitations

The design and analysis portion of this project focuses on the structural characteristics and performance of the rim. FEA simulation is performed on the geometries of the rim assembly only. Consequently, there is no detailed analysis of interaction from tire or other suspension components. Due to budget and time constraints, manufacturing resources and facilities are limited to those available in the JMS lab and ME machine shop. Due to these limitations the composites manufacturing process is performed manually. Similarly, testing resources are also limited. For this reason, simple tests using an MTS machine and the JMS race car are employed.

1.3 General requirements

Section T6.3 of the Formula SAE Rules [1] outlines the requirements for the wheels of FSAE vehicles. There is not much regulation on the wheels, but the most significant rule described pertaining to the scope of this thesis is that “the wheels of the car must be 203.2 mm (8.0 inches) or more in diameter”. More important are the requirements that arise from developing a rim that will fit the current JMS14 race car suspension design. The suspension of this vehicle is designed for a nominal 13 inch diameter wheel, meaning the rim must properly fit the current 3 inch center-lock hub, and provide sufficient clearance for the suspension components housed inside the wheel, such as the hub, upright, and brake assembly. Additionally, the rim must be designed to properly fit 20.5 x 7.0-13 inch Hoosier tires. The manufacturer recommends that the rim width for these tires be between 5.5 and 8.0 inches [2]. A proper tire bead profile must also be designed into the rim in accordance to the 13 inch wheel specifications of The Tire and Rim Association [3].

2 Background

In this chapter, fundamental concepts pertaining to the thesis are described. An understanding of basic vehicle dynamics as well as general composite materials behavior is important. Relevant information can be found in references [4, 5] and [6,7], respectively. A standard Cartesian coordinate system, seen in Figure 2.1, is used throughout this thesis to describe the directions of forces and motion with respect to a vehicle.

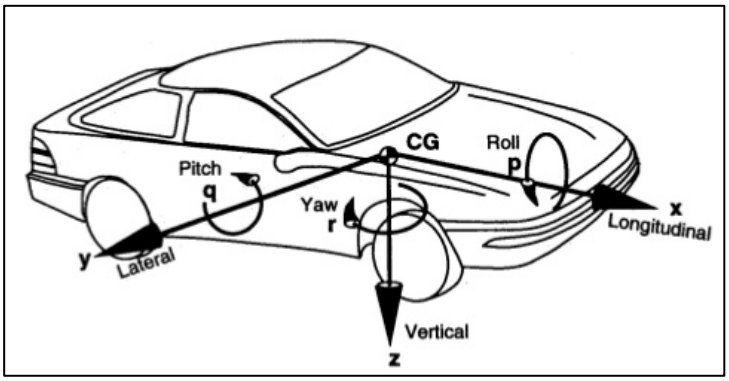

Figure 2.1: SAE standard fixed vehicle coordinate system [8]

2.1 Vehicle Dynamics

Generally speaking, vehicle dynamics is the study of a vehicle's motion based on distance, velocity, and acceleration with respect to the car's coordinate system as previously depicted. Ultimately, race engineers develop their car's design to optimize its acceleration capabilities which improves overall performance and lap times.

2.1.1 Significance of wheel mass

As is the case with most components, the mass of the wheels can have a significant effect on the vehicle dynamics and performance of a race car. The simple concept of Newton's second law provides quick proof of this; in general, if a vehicle's mass is reduced it can accelerate more quickly. Going beyond affecting overall vehicle weight, the wheels have additional significance as a rotating and unsprung mass.

As a rotating mass, the wheels affect the car's longitudinal motion with regards to their rotational acceleration. Longitudinal motion can be described by an equilibrium equation that combines the car's driving forces and resistances in the longitudinal direction, expressed as [9]:

$$F_{drive} = F_{R,air} + F_{R,roll} + F_{R,grade} + F_{R,acc} \qquad (2.1)$$

Here, F_{drive} is the driving force applied by the car's power train and the terms on the right side represent the resisting forces and are further described in Table 2.1. As written, the car is in constant velocity motion when the driving force is equal to the sum of resisting forces. In order to accelerate, the driving force must be greater than the resisting forces. Inversely, for deceleration to occur the sum of the resisting forces must be greater than the driving force.

Table 2.1: Resisting forces to longitudinal motion

Symbol	Resistance Force	Description
$F_{R,air}$	Aerodynamic Resistance	- Resistance due to aerodynamic drag
$F_{R,roll}$	Rolling/Frictional Resistance	- Resistance from tires rolling on surface - Frictional resistance from moving components such as power train, transmission and suspension
$F_{R,grade}$	Grade Resistance	- Resistance due to gravity on inclined road surface
$F_{R,acc}$	Acceleration Resistance	- Resistance from all rotating components due to their rotational inertias

It is in the final term, $F_{R,acc}$, where the weight of the wheels can impose a significant effect on the acceleration of the vehicle. Being that the wheels are relatively large in size it is important to maintain a low mass in order to reduce their rotational inertia, or moment of inertia. Doing so will reduce the required force necessary to accelerate the wheels rotation. That means that the car can accelerate and decelerate (brake) more quickly and with less effort, ultimately improving its driving performance and response to driver input. This relationship is expressed in the following equations:

Moment of inertia for a disk: $$I = \frac{1}{2} mr^2 \qquad (2.2)$$

Rotational acceleration: $$T = I\alpha \qquad (2.3)$$

In race car design, reduction of wheel weight, and thus of the unsprung mass, is also highly desirable as it is beneficial to the improvement of handling. Unsprung mass is the mass of the components that are directly mounted to the car's

suspension, rather than supported by it. These components include, but are not limited to wheels, tires, hubs, uprights, outboard brakes, suspension links, and so on. A lighter unsprung mass reduces the workload necessary from the shocks and springs to maintain consistent tire-to-surface contact, especially over road surface imperfections or changes. This means the suspension of the vehicle can provide more constant grip as well as quicker response and reaction to the wheel's vertical motion. In turn, this also provides more clear feedback to the driver.

Another area where reduction of wheel mass can provide improvement is the vehicle's yawing moment of inertia, I_z (in-lb-sec^2), which is the moment of inertia acting at the vehicle's center of gravity about the vertical, Z, axis. Simply put, the yawing moment of inertia provides resistance against changes in direction or rotation about said axis. So, the larger the magnitude of I_z, the greater the resistance to steering input making the responsiveness of the racecar seem more sluggish. Reduction of mass of components away from the CG of the car will decrease the moment of inertia. Because of their location at the extreme corners of the FSAE car, significant weight reduction of the wheels can noticeably affect a decrease in overall yawing moment of inertia. Ultimately this will lead to a more responsive racecar that can turn very quickly. This behavior is favorable for FSAE and other forms of open-wheeled racecars because they must be maneuvered around narrow tracks with tight corners. On the other hand, production consumer vehicles and large trucks will have a much higher yawing moment of inertia, but this can actually be desirable in such cases because the lower responsiveness makes the vehicle feel more stable and smoother to drive.

2.1.2 Tires

The tires provide the only contact between the race car and the road surface, thus, all of the forces required to support the vehicle's vertical weight as well as accelerate the car occur at the tires. They are the main source of the forces that ultimately affect the vehicle's overall handling [4]. These forces originate primarily at the center of the tire's contact patch on the horizontal road plane (the area of the tire that is physically in contact with the road surface) and act in either the longitudinal or lateral direction, or both. Friction between the tire and the road control the magnitude of the forces, and it is the coefficient of friction, μ, which dictates the amount of grip available to the tire. Coefficient of friction is described as a ratio of forces, F, in the longitudinal or lateral directions with respect to the applied vertical force (see Eqn. 2.4 [9]).

$$\text{longitudinal: } \mu_x = \frac{F_x}{F_z} \qquad \& \qquad \text{lateral: } \mu_y = \frac{F_y}{F_z} \qquad (2.4)$$

Race car tires are, in general, developed to produce the highest possible force capabilities in order to improve their accelerations. Of course there are many different types of tires produced that offer just as many different performance characteristics. FSAE racing tires, as well as many other kinds, are tested on special testing machines such as those at the Calspan facility used by the "Tire Test Consortium" (TTC). The TTC is organized by a number of universities that fund tire testing in order to obtain important performance data from tires in different setups [10]. The results provide insight on the effect of changing parameters such as loads, speeds and suspension geometry. This tire data can then be used by race car engineers to

determine tire performance and provide important design details such as the possible maximum forces generated by the tires for a specific vehicle setup. It is these maximum force values that are ultimately used to aid in the design of various components, as will later be described for the design of rims in this thesis.

2.1.3 Camber

As is the case with many aspects of race car design, handling and tire performance is dependent on a number of factors with regards to vehicle design and set up. An important parameter for this is the wheel and tire's camber angle. Camber angle is defined as the angle between a titled wheel plane and the vertical [4], and is considered positive if the wheel leans outward at the top relative to the chassis or vice versa. Maximum cornering force is possible at some small value of negative camber due to camber thrust, which is "caused by the straightening out of the arc of the contact patch as the tread of a cambered tire rolls over the ground" [5]. Inversely, if positive camber is induced, then cornering power can decrease. However, too much camber will lead to the tire riding on one edge of its tread, decreasing the contact patch area and changing the pressure distribution. This will diminish cornering power and may lead to excessive non-uniform tire degradation. Each tire has its optimal performance zone that largely depends on its temperature, contact patch area and pressure distribution. Although modern tire manufacturers aim to develop tires less sensitive to these parameters, the camber angle does affect these values.

Normally, camber angle is set statically but it is important to understand that the camber of each tire will vary dynamically as the race car moves around the track.

Unfortunately, it is difficult for engineers to control this [5]. That is why it is important to reduce compliance within the suspension and wheel assembly in order to lower the possibility of unpredictable and undesirable camber change. For this reason, wheel stiffness is of great significance in this matter; if the rims experience high deflection under load, then that will inherently add to unpredictable dynamic camber change, potentially harming overall on-track performance and handling.

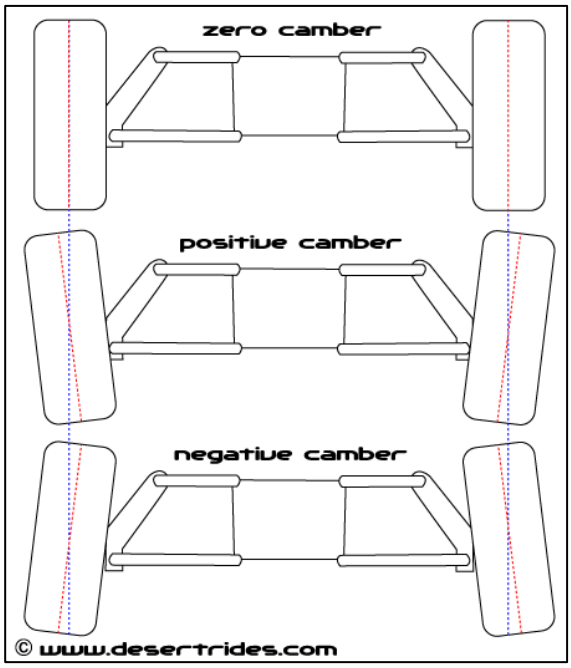

Figure 2.2: Representation of camber angle

2.2 Composite Materials

A material is considered a composite if there are two or more materials that are combined on the macroscopic level to develop a third material [6]. Composite materials are usually designed to exhibit the best qualities of its constituents and/or new qualities altogether. Some of the most valuable characteristics of composite

materials that show potential improvement over conventional metals include specific strength and specific stiffness. Composite materials can also have major differences in mechanical behavior as compared to conventional engineering materials (i.e. metals, plastics, etc.). Conventional engineering materials are most commonly homogenous and isotropic, whereas composite materials can be inhomogeneous and anisotropic. Engineers study the micromechanics and macromechanics of these materials to understand and tailor their mechanical behavior to fit the requirements of their designs.

Of course, this broad definition means that the list of composite material possibilities is endless, but there are four commonly accepted general types: fibrous, laminated, particulate, or some combination of those three. The scope of this thesis focuses on the use of laminated fiber-reinforced composite materials in a plastic matrix, or laminated fiber-reinforced plastic (FRP). This form of composite material is popular in applications that seek development of lightweight yet strong and/or stiff structures, especially in aerospace and automotive racing.

2.2.1 Laminated fiber-reinforced plastic (FRP)

For the purposes of this thesis, FRP laminates are made up of layers, or laminae, of long continuous fibers in a unidirectional or woven arrangement and in a plastic matrix. See Figure 2.3 for an example of these lamina types. In these laminae, the fibers are the principal load-carrying constituent and the matrix provides support, protection and a means of distributing and transferring loads between the fibers. Laminates are simply stacks of laminae bonded together. The orientation and specific material type of the stacked laminae can differ to provide various possibilities of

macromechanical behaviors. It is also important to note that these laminated FRPs conventionally exhibit orthotropic and linear-elastic behavior, which will be discussed later.

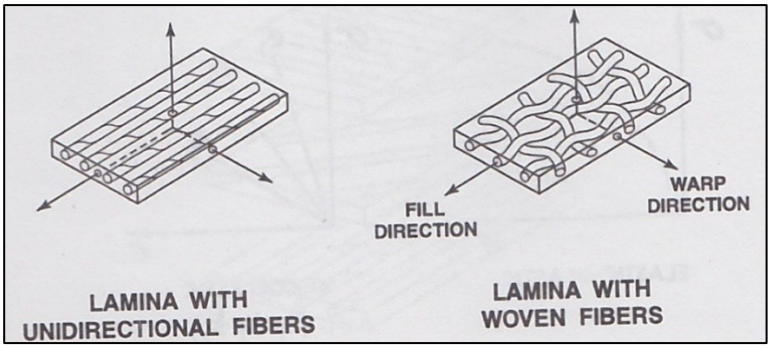

Figure 2.3: Two principal types of laminae [6]

Some of the most commonly used FRP material choices include glass, aramid, carbon and boron with epoxy matrix. A generalized comparison between the basic characteristics of these composites and more conventional materials can be seen in Figure 2.5 which illustrates why these materials are often desirable. In addition to benefits in mechanical properties and the other characteristics mentioned in Table 2.2, FRPs can be molded to produce parts with complex geometries; sometimes more easily than in common manufacturing methods of metals or other conventional materials.

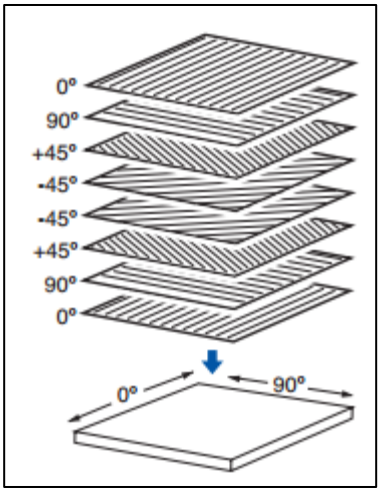

Figure 2.4: Example of a laminate

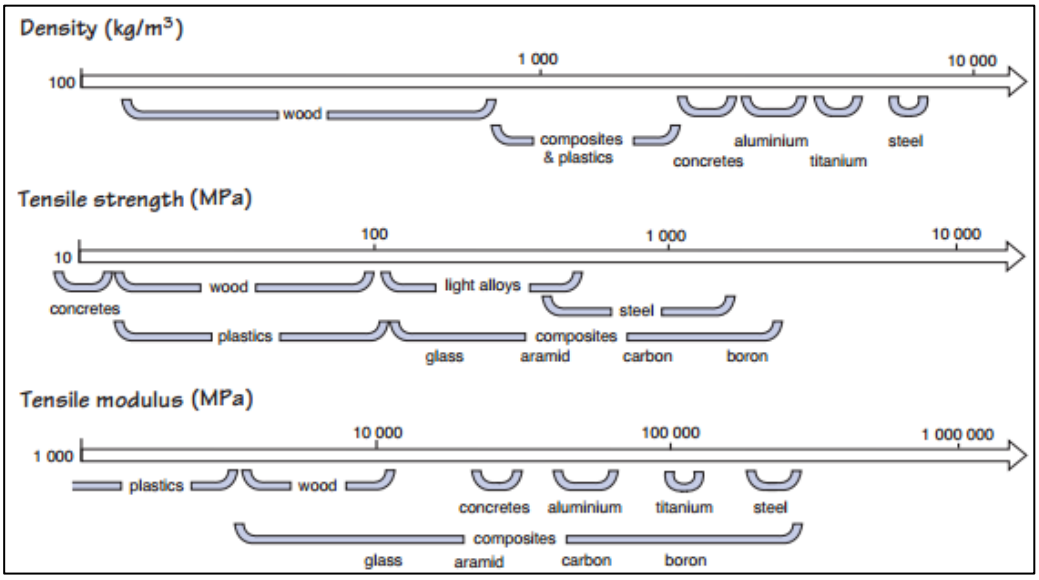

Figure 2.5: Comparison of different material characteristics [11]

2.2.2 Carbon Fiber Reinforced Plastic (CFRP)

For the development of a composite rim described in this thesis, the choice was made to use carbon-epoxy fiber reinforced plastic, or CFRP. Carbon fibers are widely used in the aerospace and automotive racing industries, mostly due to their characteristic high specific strength and chemical resistance. Manufacturers are able

to produce carbon fiber material with a wide range of stiffness and strength values, more so than for other fiber materials. In general, carbon fibers are usually on the higher end of stiffness range for fiber composites and they can exhibit relatively high strengths. Having a high stiffness-to-weight ratio makes carbon fiber material a great choice for racing wheels. Carbon fiber material is normally readily available thanks to its popularity, and the JMS team has access to different types, as will be discussed in the following chapter. The major limiting factor is the material's cost, which can be staggeringly higher than that for glass fibers or more conventional materials depending on the specific material type chosen. So, the use of carbon fiber is only economically practical in instances where weight savings provide a large payoff and it "is used as an enabling material rather than a substitution material" [7].

CFRPs, similar to other FRPs, are available in different forms, each of which has its own strengths and weaknesses as well as manufacturing methods. A few of the most common forms of carbon fiber are tow, tape, and fabric. Tow can be simply described as yarn on a spool, and is often used in pultrusion and filament winding; a popular choice for tubular shapes. Carbon fiber tape usually comes as a roll of unidirectional fibers arranged in a thin sheet that is preimpregnated with resin and held together with removable backing material. In this form, the CFRP is wound or, more commonly, laid. Fabric, or cloth, is perhaps the most traditionally recognizable form of carbon fiber, and as its name suggests, the carbon fibers are generally arranged in a thin cloth form, woven as tows (giving the popular checkered appearance), and packaged in a roll. Fabric is most commonly laid or molded and can be either pre-impregnated or dry.

2.3 Current Technologies

When it comes to making a decision about wheel choice, FSAE teams have two options: purchase rims or develop their own, the former being more popular by far. This section will describe some of the available FSAE options for purchase as well as some current technologies in the development in composite automotive rims.

2.3.1 Available FSAE wheels

The most popular wheels purchased by FSAE teams are made of metal; most commonly aluminum, but some use steel and a few are running magnesium. In general, these wheels seem to offer relatively acceptable performance. The popular aluminum options do offer a number of advantages, mainly being economically practical and relatively lightweight. However, it should be noted that many manufacturers do not develop these wheels specifically for FSAE. Instead, many of the commercially available rims used are sold by large wheel manufacturers offering options that happen to be the right size for FSAE tires; usually 10 or 13 inches in diameter and 5 to 8 inches in width. The downside to this is that the mass produced wheels are not optimized to the specific FSAE car(s) in question. Among the most widely used aluminum wheels in FSAE are those made by the company Keizer Wheels which are sold as FSAE specific rims. It is for this reason that the Keizer center lock wheels are used as a benchmark for rim development in this thesis. The Keizer wheel features a 3-piece design with an outer and inner aluminum shell and an aluminum center, assembled with several fasteners. This modular design concept makes it easy to offer different overall size and backspacing options, and they are marketed as one of the lightest aluminum options on the market. For a 13 x 6.5 inch

wheel, which could be used on the JMS FSAE car, the stock overall weight is 7.9 lbs. On average, the CL-1 wheels cost $375 each and this model is illustrated in Figure 2.6.

Figure 2.6: Keizer 13" Formula CL-1 Wheel [www.keizerwheels.com]

There are a number of FSAE teams including JMS that, understanding the significance of wheel weight, decided it would be worth the effort to develop their own wheels that are lighter than these aluminum rims. Many of these independent rim designs are made with composite materials, especially CFRP, and have proven to be lighter than purchased aluminum wheels while maintaining sufficient or higher strength and stiffness. Beginning in 2006, the JMS team developed a two-piece wheel system that it continues to use successfully with some design improvements each year. The two pieces are a carbon fiber rim shell and an aluminum wheel center, somewhat similar to the Keizer, and fastened together with nuts and bolts. The 2014 version of the 13 inch JMS wheel weighs about 4.35 lbs overall,

significantly lighter than the Keizer aluminum option. The 2014 version of the 13 inch JMS wheel is illustrated in Figure 2.7.

Although this design has been used rather successfully for some time, the need for fasteners, the relatively large aluminum center, and a thick attachment flange on the shell means that there is weight that can still be shed. For this reason, a single piece composite rim with no fasteners is investigated in this thesis.

Figure 2.7: 2014 JMS wheel

2.3.2 Composite wheel technologies

In the professional racing and high performance auto industry, there is a limited number of companies that manufacture single piece carbon fiber wheels. These are extremely lightweight and effective as compared to conventional automobile wheels, but they are expensive and do not offer options suitable for FSAE teams. There are just a few teams that have successfully developed and utilized their own single piece composite rims, but they are quite impressive and very lightweight.

These designs generally feature a 3 or 4 spoke design and normally the composite is molded as a single piece. Externally, the spokes on the rim seem to be hollow but usually this is not exactly the case. Some of the most recognized FSAE teams that run these wheels, which all happen to be European, include TU Graz, UAS Graz, and KA Racing. An example of this type of wheel is shown in Figure 2.8.

Figure 2.8: UAS Graz Racing single piece rim [www.joanneum-racing.at]

Aside from being aesthetically pleasing, these lightweight wheels have been used effectively for a few years. Although these teams keep most details of their proprietary designs confidential, some of their designers have described very general and basic manufacturing methods publicly. For instance, a major factor in manufacturing is the molding and layup of the spokes. In some designs, the spokes are laid in a female mold and a permanent core insert, usually lightweight foam, is used to form the spoke, and is left in the finished product. Another method involves the use of a pressurized bladder, made from bagging material or something similar. As in the case with the core, the bladder, which is still very lightweight, is often left

trapped inside of the spokes. Now, although these methods have been proven techniques, there are a couple of disadvantages. One downside is the fact that these methods add some weight to the wheel as compared to a completely hollow spoke. The main disadvantage though is that these spoke forming/molding methods are not reusable as the core inserts and pressurized bags have to be remanufactured for every single wheel made. This can become time consuming and costly since, in most cases, teams manufacture several wheels each season. The costs can be amplified if rims are destroyed or are not manufactured properly and replacements or repairs are required. For this reason, a cleaner and more efficient manufacturing method is explored.

As previously mentioned, there are professional composite wheel manufacturers and each utilizes its own proprietary design and manufacturing methods. Similar to the FSAE teams, the companies keep details of their designs very confidential which is, of course, good business practice, and likely the reason that there are so few such companies out there. There is however, a limited amount of publically available information from some of these businesses. One company that has provided some information in an internet article is Blackstone, the manufacturer of carbon fiber wheels for racing motorcycles. Blackstone produces wheels with hollow spokes using aluminum molds and a trapped rubber tooling technique [12]. This creates a finished product that meets the manufacturing goals of this thesis project so a similar method is ultimately used for the single piece FSAE wheel developed herein.

Other companies that have developed street legal carbon fiber rims include Carbon Revolution and supercar manufacturer, Koenigsegg. Both companies have patented hollow spoke designs as well. Through research of their products, it is clear that both utilize relatively standard layup methods and aluminum molding, similar to that currently used by JMS and Blackstone. The manufacture of the hollow spokes seems to differ from the reusable trapped rubber technique of Blackstone but no information on this is provided. In the case of Koenigsegg, it seems that a soluble trapped core may be used. Figures 2.9, 2.10, and 2.11 provide images of the Blackstone, Koenigsegg, and Carbon Revolution wheels, respectively.

Figure 2.9: Blackstone motorcycle wheels [www.sportrider.com]

Figure 2.10: Koenigsegg wheel [www.hotdigitalnews.com]

Figure 2.11: Carbon Revolution wheel [www.carbonrev.com]

3 General Design

This chapter provides an overview of the general design for the new 5-spoke composite rim developed in this thesis. The main focus here is the geometry and shape of the wheel, whereas the laminate design will be covered later in the analysis chapter.

3.1 Design Requirements

As was briefly described in the introduction, FSAE regulations [1] regarding wheels are open-ended with the main requirement being that wheels must be at least eight inches in diameter. However, for the purpose of the wheel developed for this thesis project, the most significant requirements come from application to the current JMS racecars. The wheel must fit the cars' current configuration, meaning it must mount using their 3" center lock hubs and nuts with the correct drive pin pattern. There must also be correct backspacing (described by Figure 3.1) and sufficient clearance for packaging of the components that are essentially housed inside the wheel including the hub, upright, brake rotor and brake caliper as seen in Figure 3.2. Additionally, the cars targeted for this rim run 13" rim diameter Hoosier tires that are 7" wide, so the wheels need to be properly sized to fit these.

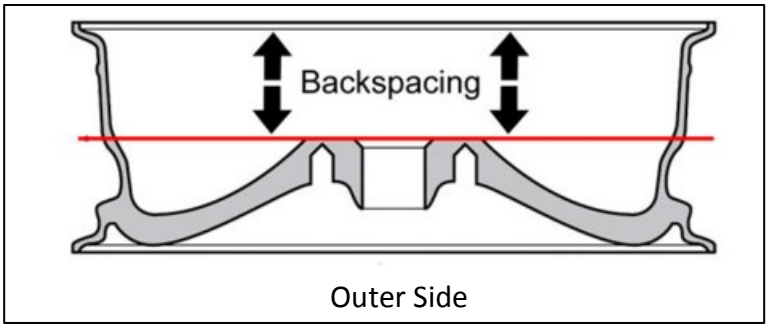

Figure 3.1: Wheel backspacing [www.usedtiresintexas.com]

Figure 3.2: Components packaged inside of wheel

3.2 Five Spoke Wheel Design

Given the goals of developing a lighter, single-piece composite rim and given the design requirements as well as time and resource constraints, the choice was made to revive and repurpose a previously designed single piece composite wheel concept.

3.2.1 Original design concept

This five spoke wheel was originally designed in 2006 and prototypes were made by a JMS team member at the time. However, the design was never successfully implemented mainly due to difficulty of, and failures in, manufacturing as well as a switch from a 4-lug hub to a center-lock hub design. So, because JMS was already in possession of the large aluminum molds used to create the old 5 spoke rim, and the wheel is of correct general dimensions, it was decided to modify its design to fit the needs for current JMS racecars and this project. Making this choice greatly decreases the amount of time required for design conceptualization and, more significantly, manufacturing time and resources. Aside from the time and resource benefits for the scope of this project, the design is a good choice because it is already slightly lighter than the current 2-piece rims, and the five spoke design should provide sufficient load distribution and structural integrity to the rim. Not to mention, this design is also aesthetically pleasing. The 2006 5-spoke wheel is pictured in the Figure 3.3 below.

Figure 3.3: 2006 5-spoke wheel

3.2.2 New design modifications

As mentioned, design modifications are required to make this old wheel concept work for the purpose of this thesis and, ultimately, for the use on current JMS vehicles. There are two main areas that require redesign: the center mounting section and the tire bead profile around the rim hoop. A bead profile is designed in accordance to the TRA profile specifications [3] for a 13 inch diameter wheel. Following this standard design should allow for correct tire sealing and fitment. The wheel center, however, required more thought and consideration. Since the spoke section of the rim is hollow, manufacturing had to be carefully considered. It was decided that a center insert would be made to accommodate the center-lock system that will be bonded into the center of the spoke section of the wheel, replacing the original 4-lug design. The design for the center piece used throughout this thesis project is shown in Figure 3.4. It is simply a round aluminum piece with the appropriate angled nut face and drive pin holes to accommodate the current center-

lock mounting system. Aluminum was chosen for the insert because it is less vulnerable to abrasion from hub nut torqueing than carbon fiber and is quicker to manufacture. Both the inside and outside spoke center faces get large circular holes in them to fit the aluminum insert appropriately. Drive pin holes are added to the inside face so that the drive pins on the hub will pass through both the composite and the aluminum. Tabs are added to the inside of the of the wheel's center section as a means to bond the circumference of the aluminum insert. These tabs are designed to be of sufficient bonding area while being small enough and located such that the hollow spokes can be manufactured as is described in Chapter 6. Ultimately, the aluminum insert slides in and is bonded to both the inside face and the circumferential tabs. It is also designed so that the inside composite skin ends up sandwiched between the aluminum insert and the hub upon mounting on the vehicle. This approach should allow for a safe and positive locking assembly, since upon mounting to the vehicle the insert and rim are mechanically fastened together in addition to the epoxy adhesive used to bond the pieces together. The remainder of this section provides further insight to the design modifications discussed for the newly developed wheel.

Figure 3.4: Aluminum center-lock insert

The piece pictured in Figure 3.4 is the bonded aluminum insert. Note that the outside face has a large angled feature to properly fit the angle of the current center-lock nuts used on JMS cars. The holes on the inside face of the insert are positioned so that the drive pins on the hub will fit right inside of them. Because of the center-lock design, the purpose of the drive pins is to transfer the rotation between the wheel and the hub. This creates a more reliable engagement than that of solely depending on the contact pressure and friction from tightening the nut onto the hub – which by itself can lead to slippage and therefore damage to the wheel and/or hub. Pockets on the inside end are cut for weight savings while maintaining a conservative amount of bond area. As calculated by the FEA model, later described in Chapter 5, the modeled weight of the wheel using the laminate described in chapter six (not including extra bead layers or epoxy) is 2.95 lbs.

Figure 3.5 depicts the modified hollow composite center section, where the aluminum center simply slides in and is bonded onto the circumferential tabs onto the inside skin of the rim. The drive pins will pass through both the composite skin and

the aluminum, helping prevent the occurrence of high torsional shearing stresses between the two pieces. This means that the adhesive bond is only partially carrying the loads experienced in this region. In order to determine that there is sufficient bond surface area for the Hysol epoxy chosen, simple conservative hand calculations were conducted and are included in the appendix.

Figure 3.5: Hollow composite wheel spokes

Figure 3.6: CAD model of 5-spoke rim

3.3 Design Discussion

As was mentioned, the approach of revamping a previously designed geometry has its definite benefits. However, additional design modifications can be considered for future development efforts that may be of benefit. For instance, as a rule of good practice with composite laminates, radii within the geometry could be enlarged to avoid sharp edge features and reduce the potential severity of stress concentrations in those areas. Also, the valley feature around the wheel's hoop could be revisited. Although this geometry is dictated by the TRA standard [3], a more gradually sloped profile may help increase structural integrity around the rim. The purpose of that valley feature is to allow for proper installation and removal of the tire, so that must be carefully considered if design changes are pursued. Regardless of the modifications considered, it is important to ensure that the components housed inside the wheel will still be neatly packaged, as there is little clearance to begin with.

Design changes to the base geometry of the hoop or spokes would likely prove costly and time consuming. At a minimum, more complex machining will be necessary to modify the existing aluminum tooling, or perhaps the complete redesign and manufacture of new tooling may be required. So, for the scope of this thesis project, it was decided that these apparent costs outweighed the potential benefits of further geometric design modifications.

4 Materials

As is the case with the development and production of any structure, materials and their properties are among the most significant driving factors in the design process. For this reason, material selection must be given ample consideration to make an effective choice for the project at hand. This chapter will discuss the materials used throughout this project.

4.1 Material Selection

When it comes to an automotive wheel, there are a number of material options that can be used to create a product that serves the basic function. Currently, the most conventional materials used for wheel production are metals like steel or aluminum, and generally these materials work just fine for most road cars and production vehicles where optimizing handling and high-speed driving performance may not be the most important goal, unlike the case for racecars. However, when weight reduction is a significant factor for racecars, as explained in Chapter 2, it seems that the lightest metallic options have plateaued in terms of reaching minimum weight while still providing necessary strength and stiffness. It is for this reason that composite materials are considered as an alternative throughout this thesis. In

particular, CFRP is chosen for development of the new FSAE racing wheel due to its high stiffness-to-weight ratio.

4.1.1 Choosing the specific CFRP

There are many types of CFRP that are commercially available and general details were provided in Chapter 2. For this project, the specific materials available are those that are currently in the possession of the JMS FSAE team. From these options it was decided to use pre-impregnated (prepreg) carbon fiber material. A prepreg material is a fiber reinforced resin matrix that comes ready to use in manufacturing, unlike more traditional wet-layup materials that require the resin matrix to be mixed and applied to the dry fiber fabric during manufacturing. This allows for a cleaner, more efficient layup process. Because the resin is pre-impregnated into the fabric, the resin/fiber volume ends up being much more consistent and closer to ideal than manually mixed and applied wet-layup resin. Ultimately this can provide a finished product of higher quality, with better controlled layup and potentially shorter manufacturing times. Of course, being a superior form of CFRP, prepreg carbon fiber is generally much more expensive than its less advanced alternative. Even though that is the case, the JMS team already utilizes prepreg for several structures on the car and it has sufficient resources to support this project, making prepreg CFRP a feasible choice.

JMS gets material from a few different suppliers, most commonly from manufacturers Cytec, Park, and Gurit. During the time of this project, the most abundant materials in stock were from Park and Gurit, so it was decided that the CFRP to be used would come from one or a combination of these manufacturers.

The specific composites available from these manufacturers and some of their mechanical properties are listed in Table 4.1.

Table 4.1: Prepreg CFRP material options [13-16]

Description	E_1 (msi)	F_{1t} (ksi)	Thick. (in)
Park E765 / T300 3K PW	8.1	89.0	.009
Park E765 / T300 6K 5HS	9.3	86.1	.015
Park E765 / T700 24K Uni	19.0	370.2	.006
Gurit SE70 / HMC300 Uni	30.2	226.5	.012

Stiffness is a driving factor of the wheel design, so iterations of laminate options are reviewed using these different materials (details in Chapter 5, Table 5.5). It is determined that a combination of unidirectional and woven fabric should be used to satisfy common rules of practice in composites manufacturing. For instance, it is a good idea to place a ±45° woven layer on the outside surfaces of a part to increase wear and damage tolerance, as well as reduce possibility of fraying. Due to its high stiffness, the Gurit SE70 / HMC300 uni is chosen as the prominent lamina option for the new wheel design, and Park E765 / T300 3K PW is chosen as the woven cloth option mainly because it is lightweight, while still providing sufficient stiffness. It should be noted that high-modulus carbon (HMC), such as the Gurit material, is considered more of a specialty product and is much more costly than a standard modulus material. However, since the material is readily available to JMS and high stiffness is of such importance, the Gurit material is a good choice.

4.2 Material Properties

In this section, the mechanical properties of the materials selected are discussed along with testing methods to verify their respective manufacturer provided data.

4.2.1 Manufacturer's data

The following tables provide the manufacturer's mechanical properties data for both the Gurit and Park CFRP materials chosen.

Table 4.2: Park E765 / T300 3K PW manufacturer properties from test data [13]

E_1 (Msi)	8.20
E_2 (Msi)	8.01
v_{12}	0.059
G_{12} (Msi)	0.56
G_{13} (Msi)*	0.524
G_{23} (Msi)*	0.524
F_1^t (ksi)	90.46
F_1^c (ksi)	96.31
F_2^t (ksi)	77.82
F_2^c (ksi)	87.52
F_{12} (ksi)	18.86
F_{13} (ksi)	10.38
V_f	0.5

*Estimated from comparison of similar material [17]

Table 4.3: Gurit SE70 / HMC300 Uni manufacturer design properties [16]

E_1 (Msi)	30.2
E_2 (Msi)	0.927
v_{12}	0.337
G_{12} (Msi)	0.625
G_{13} (Msi)	0.625
G_{23} (Msi)**	0.259
F_1^t (ksi)	226.5
F_1^c (ksi)	122.3
F_2^t (ksi)	4.17
F_2^c (ksi)	12.05
F_{12} (ksi)	9.38
F_{13} (ksi)	9.38
V_f	0.56

**Estimated using the equations below

Calculation of G_{23} for unidirectional material using the following relationship from the Chamis model [33]:

$$\nu_{23} = \frac{E_2}{2G_{23}} - 1$$

So:

$$G_{23} = \frac{E_2}{2(1+\nu_{23})}$$

From Rule of Mixtures [34]:

$$\nu_{23} = 1 - \nu_{21} - \frac{E_2}{3K}$$

$$K = [\frac{V_f}{K_f} + \frac{(1-V_f)}{K_m}]^{-1}$$

$$K_f = \frac{E_f}{3(1-2\nu_f)}\,,\; K_m = \frac{E_m}{3(1-2\nu_m)}$$

Where the following values are provided for Gurit SE70/300 HMC uni, except for the fiber and matrix Poisson's ratios which are assumed from common unidirectional carbon fiber properties:

$$\nu_{21} = 0.01014\ ;\ V_f = 0.56\ ; E_f = 55.84\ Msi\ ;\ E_m = 0.52\ Msi\ ;\ \nu_f = 0.3\ ;\ \nu_m = 0.375$$

Upon calculation:

$$K_f = 46.53\ Msi\ ;\ K_m = 0.693\ Msi\ ; K = 1.546\ Msi\ ;\ \nu_{23} = 0.79$$

$$G_{23} = 0.259\ Msi$$

Now, this is a simple calculation for the G_{23} property of the unidirectional lamina using isotropic bulk modulus due to lack of specific material properties, which could lead to inaccuracy. The interlaminar shear stiffness is also dependent on the stacking sequence of the laminate [36], which is not captured here. For these reasons, a quick sensitivity study is performed to determine whether or not variation in G_{23} assigned to the Gurit uni will lead to a significant change in the structural performance of the wheel. For this study, G_{23} values of 50% and 200% of that calculated are run in the 5-spoke FEA model simulation under the combined acceleration and turn load case; the details of which are described in chapter 5. The effect that the variation in G_{23} has on the overall deflection and Hoffman reserve factor is shown in the table below. These results show that even a large variation does not significantly impact the overall structural performance of the wheel, so the use of the calculated G_{23} is deemed acceptable.

Table 4.4: Gurit uni G23 sensitivity study

G_{23} (Msi)	0.259	0.1295	0.518
Max. Displacement (in.) [% growth]	0.1125	0.1152 [+ 2.4%]	0.1108 [- 1.5%]
Min. Hoffman RF [% growth]	1.535	1.526 [- 0.6%]	1.540 [+ 0.3%]

4.2.2 Mechanical properties verification tests

For design and analysis purposes in this thesis, manufacturer's lamina mechanical property data is used. This is done to cut down on extensive testing time and resources, but it is necessary to at least verify to some degree that the provided data is correct and applicable since manufacturing processes and conditions can lead to mechanical property variations. In order to conduct this verification, two common ASTM standard tests are performed on specimens manufactured in the JMS lab, in a manner consistent with the process to be used for rim manufacturing. The two tests considered are the ASTM D3039 composite tensile test [19] and the D2344 composite short-beam shear strength test [20]. The tensile test is used to verify E_1^t and F_1^t values, while the short-beam shear test is used to verify the apparent interlaminar shear strength (F_{13}). Both tests are carried out using an MTS universal testing machine.

The tensile testing is performed with specimens from a single batch of each carbon fiber prepreg material since only that one batch will be used for the manufacture of the wheel prototype. Specimens are sized and manufactured in accordance to the guidelines provided in the ASTM D3039 testing standard. The Park plain weave laminate is 11 [0°/90°] layers and cured at the recommended cycle of 275°F for 2 hours. The Gurit unidirectional laminate is 3 [0°] layers and cured at the recommended cycle of 230°F for 2 hours. As recommended, fiberglass gripping tabs are bonded to the ends of the tensile specimens in order to avoid damage to the carbon fiber from the serrated gripping jaws of the test apparatus. Pictures and dimensions of the tensile specimens are shown in following figures and data tables.

Tensile gripping fixtures with lightly serrated jaw inserts are fitted onto the MTS machine to grip the specimens. In order to determine the specimens' modulus and tensile strength, load and displacement must be measured throughout the test. A vertical load cell installed in the MTS machine measured the applied load and a laser extensometer is used for precise measurement of displacement. MTS Testsuite Elite software is ultimately used for processing of the measured data. For the tensile testing, a crosshead displacement rate of .05 in/min is used. The results of the tensile tests for the woven and unidirectional materials are shown in Table 4.5 and 4.6 respectively.

Table 4.5: Park E765/T300 3K PW tensile test results

Specimen	Width (in)	Thick. (in)	$F1^t$ Meas. (ksi)	$E1^t$ Meas. (Msi)	$F1^t$ Man. (ksi)	$E1^t$ Man. (Msi)
T1	0.858	0.097	84.338	8.275	90.46	8.2
T2	0.884	0.097	90.134	8.658		
T3	0.909	0.098	87.994	8.825		
		Average	87.489	8.586		

Table 4.6: Gurit SE70/HMC300 uni tensile test results

Specimen	Width (in)	Thick. (in)	$F1^t$ Meas. (ksi)	$E1^t$ Meas. (Msi)	$F1^t$ Man. (ksi)	$E1^t$ Man. (Msi)
T4	0.492	0.034	305.884	26.475	226.5	30.2
T5	0.512	0.036	308.344	29.969		
T6	0.49	0.036	289.451	27.243		
T7	0.498	0.035	305.742	25.853		
		Average	302.355	27.385		

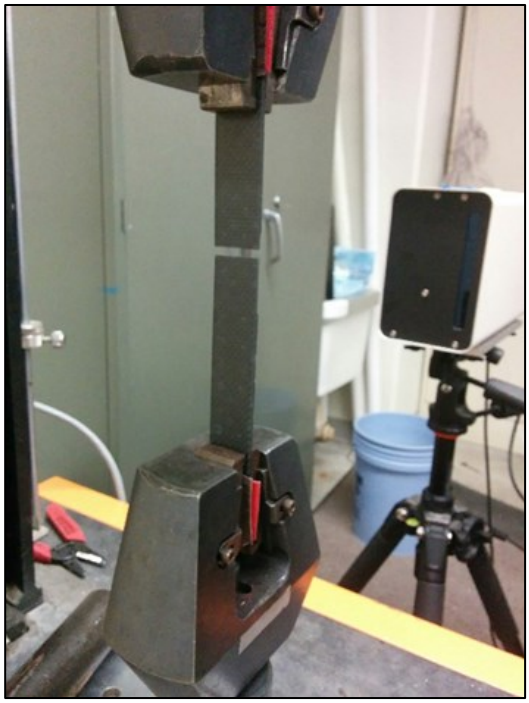

Figure 4.1: Tensile test setup

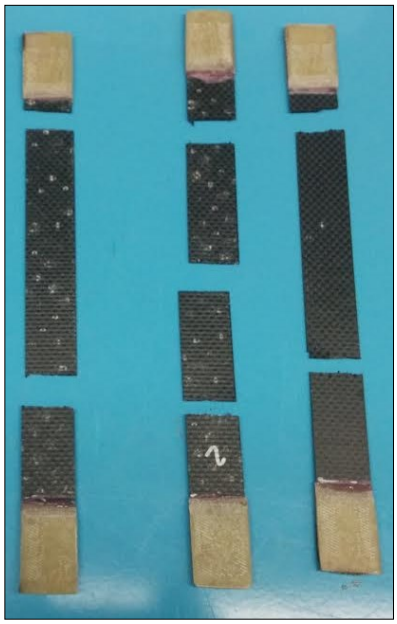

Figure 4.2: Broken tensile specimens

The tensile results for the Park plain weave material show a 5% increase in modulus and a 3% decrease in tensile strength as compared to the manufacturer's test

data, which is a reasonably close correlation. Test results for Gurit's unidirectional material do show more variation compared to the manufacturer provided properties. The measured modulus is 9% lower and the tensile strength is 33% higher. It should be noted however, that the material properties provided by Gurit were specified as design values, not test data, so it is possible their design strength value may be conservative.

The next set of testing performed is short beam shear, done according to the ASTM D2344 standard procedure. Again, both Park and Gurit prepregs are tested and the specimens are made from the same batches of material. This testing is carried out on the MTS machine using a three-point bending fixture with support pin diameter of 0.25 in. and load pin diameter of 0.5 in. The ASTM standard recommendation of a support span 4 times the specimen thickness and a crosshead compression speed of 0.05 in/min is followed. Small, flat specimens were manufactured according to the standard guidelines. A 14 layer [0°/90°] laminate was made for the Park material, and a 12 layer [0°] laminate for Gurit. The dimensions of the specimens are shown in the following results tables and were determined from the recommendations of width being twice the thickness and length being 6 times the thickness. For this set of tests, the same standard cure cycles from the tensile tests are used. During the test, the applied compressive force is measured by the MTS vertical load cell until the specimen fails. The peak applied force is then used to calculate the short beam shear strength, or apparent interlaminar strength, with the following equation [20].

$$F^{sbs} = 0.75 \times \frac{P_m}{b \times h}$$

Where:

$$F^{sbs} = short\ beam\ strength\ (psi);\ P_m = \max load\ (lbf);$$
$$b = specimen\ width\ (in); h = specimen\ thickness\ (in)$$

Table 4.7: Park E765/T300 3K PW short beam test results

Specimen	Width (in)	Thick. (in)	Span (in)	F_{13} Meas. (ksi)	F_{13} Man. (ksi)
B-P1	0.253	0.116	0.48	10.910	10.38
B-P2	0.237	0.116		8.943	
B-P3	0.24	0.116		8.979	
B-P4	0.241	0.12		10.456	
B-P5	0.24	0.118		10.874	
B-P6	0.245	0.118		10.061	
B-P7	0.245	0.12		10.421	
B-P8	0.243	0.119		9.394	
			Average	10.005	

Table 4.8: Gurit SE70/HMC300 uni short beam test results

Specimen	Width (in)	Thick. (in)	Span (in)	F_{13} Meas. (ksi)	F_{13} Man. (ksi)
B-U1	0.275	0.135	0.54	9.091	9.38
B-U2	0.275	0.134		9.220	
B-U3	0.252	0.134		9.237	
B-U4	0.274	0.133		9.191	
B-U5	0.275	0.134		9.035	
B-U6	0.271	0.135		8.813	
			Average	9.098	

These test results show that the average measured interlaminar shear strengths are approximately 4% and 3% lower than the provided properties for the

Park and Gurit materials respectively.

Figure 4.3: Short beam test setup

4.2.3 Modified cure cycle testing

It is important to note that these two chosen materials do have different types of epoxy matrices and each has different standard recommended cure cycles. The general datasheet provided with Gurit SE 70 states the material has a wide range of cure temperatures and times, from 160°F for 16 hours to 230°F for 50 minutes with typical ramp rate of 2-4°F/min [21]. A similar document from Park states a commonly used cure cycle of about two hours at 270-280°F, but also mentions a general cure temperature range of 260-350°F with lower temperature cures possible depending on the application and typical ramp rate of 1-5°F/min [22]. From prior correspondence, engineers at Park stated that a lower cure temperature of 240°F held for four hours would provide a sufficient cure for their E765 prepreg. Because the two resin matrices have different recommended cure cycles and both materials

will be co-cured for the new wheel prototype, it is necessary to determine a modified cure cycle that can be used while maintaining mechanical properties as close to standard as possible. Ideally, the shortest cure time – and therefore highest cure temperature – would be chosen to speed up the manufacturing process, but care must be taken to ensure that the matrix cures completely while also avoiding damage from excessive heat. Keeping that in mind, a cycle with target cure time of four hours at 240°F is chosen.

Further testing is performed to verify that the material properties are still acceptable for use as originally planned. As conducted, tensile testing results are dominated by fiber failure which should be relatively independent of matrix performance. Therefore, short-beam shear testing is a better choice for verification since matrix characteristics are more significant in the results and ultimately the cure cycle affects the matrix the most. So, another set of D2344 short beam tests were performed on specimens of each material, cured at the new cycle. The specimen manufacturing was based on the same specifications as in the previous short beam test, although slightly thinner laminates were used. The Park specimens were made up of 12 [0°/90°] layers, and the Gurit of 12 [0°] layers.

Results of these specimens are shown in Table 4.9 and 4.10. The Park E765 average measured interlaminar shear strength is 9.6% lower than the manufacturer's data, and the Gurit showed only a 2% decrease.

Table 4.9: Park E765/T300 3K PW modified cure short beam results

Specimen	Width (in)	Thick. (in)	Span (in)	F_{13} Meas. (ksi)	F_{13} Man. (ksi)
C-P1	0.209	0.102	0.41	9.481	10.38
C-P2	0.218	0.101		9.715	
C-P3	0.205	0.103		9.541	
C-P4	0.202	0.101		9.036	
C-P5	0.214	0.102		9.373	
C-P6	0.202	0.103		9.437	
C-P7	0.208	0.101		9.571	
C-P8	0.216	0.102		9.538	
C-P9	0.199	0.101		8.959	
C-P10	0.201	0.102		9.164	
			Average	9.382	

Table 4.10: Gurit SE70/HMC300 uni modified cure short beam results

Specimen	Width (in)	Thick. (in)	Span (in)	F_{13} Meas. (ksi)	F_{13} Man. (ksi)
C-U1	0.244	0.125	0.5	8.380	9.38
C-U2	0.256	0.123		9.142	
C-U3	0.249	0.124		9.665	
C-U4	0.259	0.125		9.181	
C-U5	0.255	0.125		8.864	
C-U6	0.245	0.124		9.255	
C-U7	0.244	0.122		9.355	
C-U8	0.26	0.122		9.474	
C-U9	0.256	0.123		9.251	
C-U10	0.255	0.125		9.447	
			Average	9.201	

Now, because the two prepreg materials are made with different epoxy matrix compounds, it is possible that the two may be incompatible for co-curing as is desired. If that were the case, co-curing the two materials in a combined laminate could lead to unfavorable curing characteristics and/or diminished structural performance. In order to determine if combining the two materials in a laminate is

acceptable, a third set of short beam tests were conducted. This time, the specimens were a laminate made up of both the Park and Gurit materials, and cured at the modified cycle of 4 hours at 240°F. The 10 layer laminate used is representative of the new wheel's design with a layup of $[0/90, 0, 0/90, 0, 0]_s$.

Table 4.11: Combined laminate short beam results

Specimen	Width (in)	Thick. (in)	Span (in)	F_{13} Meas. (ksi)
D-C1	0.226	0.1	0.43	8.924
D-C2	0.231	0.103		9.851
D-C3	0.222	0.102		8.903
D-C4	0.201	0.099		9.163
D-C5	0.239	0.103		9.754
D-C6	0.205	0.102		9.660
D-C7	0.211	0.101		9.458
D-C8	0.199	0.099		9.632
D-C9	0.219	0.102		9.539
D-C10	0.228	0.098		8.816
			Average	9.370

The results shown in Table 4.11 above for the combined laminate short beam shear testing are quite favorable, with measured average apparent interlaminar shear strength of 9.37 ksi. This value is close to the manufacturer's data of the Gurit unidirectional material, so that will be used as an acceptable strength limit for analysis. These positive results also demonstrate that both materials may be co-cured effectively, since there is no apparent significant degradation of interlaminar shear strength.

5 Analysis

This chapter provides an overview of the analysis performed to develop a laminate design for the single piece CFRP rim. In order to investigate the structural performance characteristics of the wheel, finite element analysis is used. MSC Patran and Nastran (2014) are the pre/post processing and solver programs utilized in this thesis, as this is the most commonly used FEA package in the ME department at KU. This software package is highly renowned and provides sufficient capabilities to perform analysis on both metallic and composite structures as required for this particular project.

The overall analysis process includes benchmarking of current FSAE rims to determine baseline performance targets, the development of a preliminary laminate for the 5-spoke rim, and structural analysis of that laminate

5.1 General Setup

Before discussing the details of analysis it is necessary to understand the basic model setup and load cases that are used for the FEA studies. Details are also included in the appendix.

5.1.1 Basic geometry setup

As is required in any FEA simulation, a representative geometry is necessary to create the finite element model used for analysis. CAD models of the rims to be analyzed are developed using SolidWorks 2015 software. Due to the nature of the physical wheel's design, the thin rim shell, or hoop, is simply modeled as a surface, or shell, while the wheel center is modeled as a solid body. After creating a satisfactory assembly geometry, it is imported into Patran as a parasolid file, and is then ready for manipulation and FEA model creation as is later described.

The decision to model the rim shell(s) as a shell comes from plate and shell theory [23]. In this case, Nastran CQUAD 4 elements are used in the model, which utilize Mindlin's shell theory. Plates and shells are components with small thickness compared to their length and width dimensions, allowing for reduction to a two-dimensional solid mechanics problem. Similar assumptions are also widely applied to thin composite laminates under the "classical lamination theory" [6].

Figure 5.1: Example of CAD geometry

5.1.2 Load cases

The load cases applied to the wheels were taken from the 2014 JMS tire load data, originally developed by JMS team vehicle dynamics specialists using TTC [10] tire data and suspension geometry/kinematics calculations. This car was chosen because its data was readily accessible, runs 13 inch diameter wheels with Hoosier tires, and is representative of the current JMS vehicle performance state-of-the-art. Ultimately there are five major load cases considered: maximum longitudinal acceleration, maximum longitudinal braking, maximum lateral acceleration, maximum combined acceleration and turning, and maximum combined braking and turning. Each load case consists of forces acting in the three axes of the fixed vehicle coordinate system (Figure 2.1) at the center of the tire contact patch area. These load cases are outlined in Table 5.1 and are considered limit loads for the wheel design. It should be noted, while rims for production vehicles must be designed for impact, such as striking a curb or pothole, it is not necessary in this application due to the nature of the racing environment. Generally, road racing surfaces are smooth with little chance of harsh wheel impact, but if it were to occur, wheel failure is acceptable.

Table 5.1: JMS14 wheel load cases

Load Case	Longitudinal, X (lbf)	Lateral, Y (lbf)	Vertical, Z (lbf)	Pressure (psi)
1. Max long. accel.	300	0	240	10
2. Max long. brake	-350	0	300	10
3. Max lat. accel.	0	-630	380	10
4. Max comb. accel. + turn	280	-650	380	10
5. Max comb. brake + turn	-307	-410	330	10
6. Max pressure	0	0	0	30

Note that in load cases 1-5, a pressure of 10 psi is also applied to the rim shell surface to act as the nominal operating tire pressure. The 30 psi pressure in load case 6 is to represent a maximum internal pressure that could be seen during the bead seating process of tire installation. As mentioned, these loads are originally taken directly from the contact patch of the tire. In order to mimic reality more closely, an assembly including an accurate model of the tire would need to be simulated so that tire deformation and load transfer could be included. However, for this analysis the tire loads are applied directly to the wheel geometry. Taking this approach greatly simplifies the FEA model allowing set up and run times of the simulation to be minimized. Additionally, applying the tire loads directly to the wheel creates a more conservative load case with some extra factor of safety because the energy absorption and total load distribution caused by tire deformation is not completely accounted for.

The vertical loads are applied to an area of the bead profile at the bottom of the wheel, determined by an angle calculated from the measured tire contact patch length and distance from wheel center to ground of resting car at full operating weight. The determination of the angle for vertical load application is described by Figure 5.2 below; where length is 3.75 inches and center to ground distance (R_l) is 10.125 inches, leading to an angle (θ) of 21 degrees. It is then assumed that the lateral load application area is 80 percent of the vertical load area [24], meaning a section with an angle of 16.8 degrees. Details of vertical and lateral load application are illustrated in Figure 5.3.

For the load cases with acceleration or braking, the longitudinal load is applied as a remote force acting at the center of the contact patch and tied to the entire circumference of the rim's bead profile.

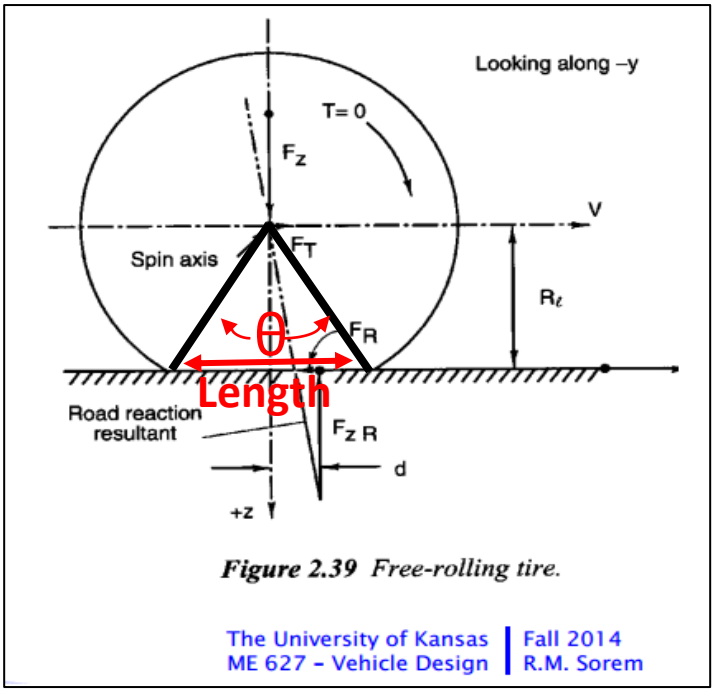

Figure 5.2: Vertical load application angle

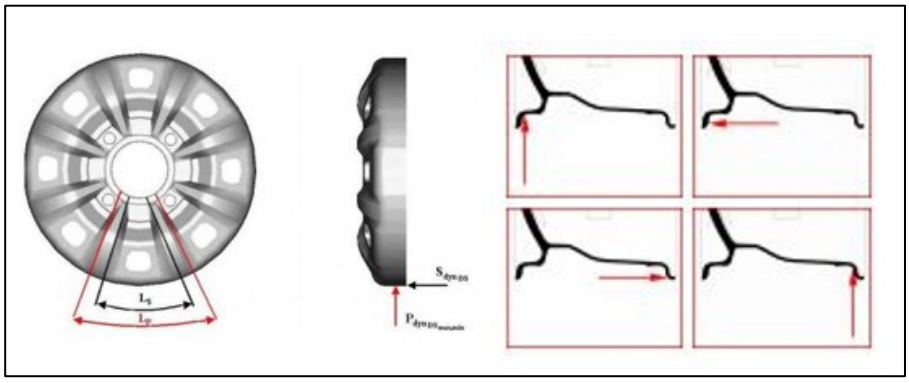

Figure 5.3: Vertical and lateral load application detail [24,25]

5.2 Benchmarking Analysis

In order to develop a new effective wheel, it is necessary to establish baseline performance targets or goals. In the case of this wheel, the primary goals are to produce a stiff yet lightweight rim with sufficient structural integrity. To obtain these performance targets, benchmarking analysis is performed on currently available rim options. Due to the lack of physical wheel testing resources, benchmarking studies are performed with FEA. This general process has been used for 9 years on other JMS rims without a single on-track failure, thus providing a high level of confidence. A commercially available aluminum wheel is simulated, and the results are used to ultimately establish a performance target for the new wheel design. Additionally, the current two piece JMS composite wheel design is also simulated for comparison purposes. During the benchmarking process it is determined that load case 4 (LC-4), which is the combined turning and acceleration case, is the most extreme condition and produces the largest amount of displacement in the rim. For this reason, LC-4 will be utilized for the benchmarking analysis discussed in this thesis.

5.2.1 Aluminum wheel

Due to its popularity, the commercially available 13 inch, center lock aluminum wheel from Keizer is selected as the performance benchmark. To start with, a CAD model provided on the Keizer website is downloaded and modified in SolidWorks, shown in Figure 5.1, to match the width and backspacing of the new composite wheel design. Additionally, the nut and bolt fasteners are removed. The geometry is then imported and the FE model is created in Patran. The wheel assembly is made up of three parts; an inner hoop, outer hoop and center, and each is made of 6061-T6

aluminum. In this study, the inner and outer hoops are meshed with CQUAD4 shell elements and the center is meshed with TET10 solid elements. Glued contact surfaces are specified at the mating flange on each of the three parts to fasten the assembly together. Load case 4 is applied to the FEA model with constraints on the wheel's center hub region, and linear-static analysis is run. The results from this study are shown in the following figures and tables. Details of the FE model setup and execution are provided in Appendix B.

The displacement values are shown in Table 5.2 and equivalent stresses along with yield and ultimate safety factors are shown in Table 5.3. These results will function as the baseline target for the new composite design. As explained in chapter 2, high wheel stiffness is important to avoid excessive dynamic camber change while driving which negatively impacts handling performance. Because the Keizer aluminum wheel is so widely used, its performance is considered satisfactory. So, under the same load conditions, the new composite wheel's maximum displacement magnitude should be less than 0.140", and its minimum safety factor (von Mises) should be greater than 1.23 to show improvement in performance and reliability. It should be noted that the safety factor herein is defined as the ratio of material yield or ultimate strength to the applied stress from FEA results. In the case of the aluminum rim, von Mises stress is measured and reported.

Table 5.2: Aluminum rim LC-4 displacements

Max Displacement Magnitude	0.140 in.
Max Displacement: longitudinal	0.061 in.
Max Displacement: lateral	-0.087 in.
Max Displacement: vertical	0.109 in.

Table 5.3: Aluminum rim LC-4 strength

Component	Max Eq. Stress (von Mises)	Min. Safety Factor (yield)
Outer hoop	11.4 ksi	3.51
Inner hoop	21.0 ksi	1.90
Center	32.5 ksi	1.23

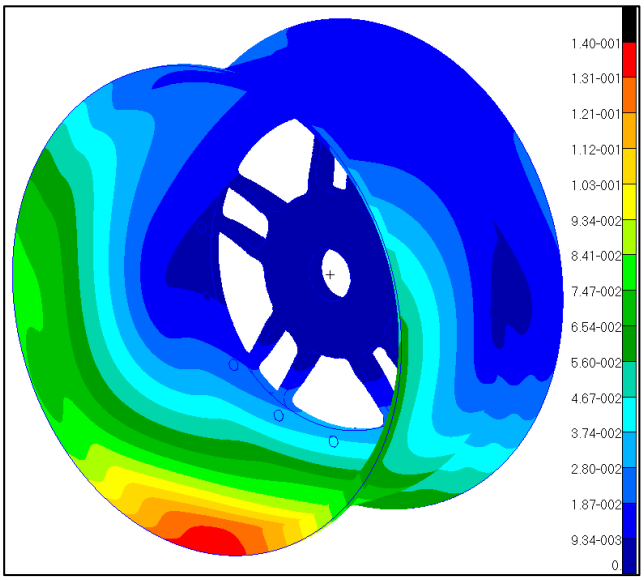

Figure 5.4: Aluminum rim LC-4 displacement magnitude

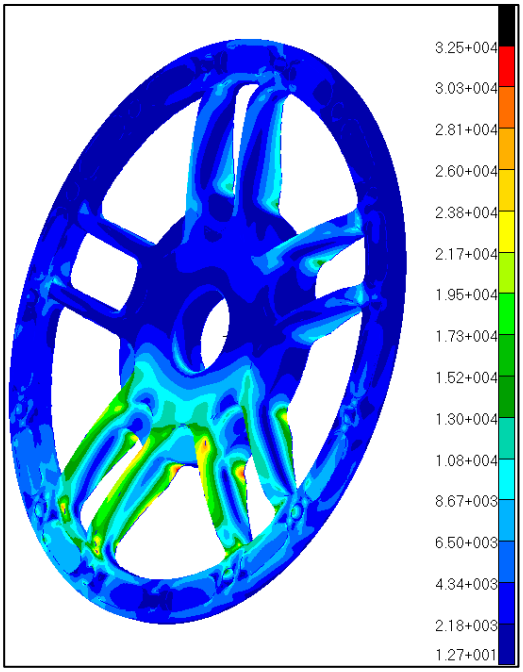

Figure 5.5: Aluminum rim center von Mises stress

5.2.2 JMS 2-piece composite wheel

The same process is used to conduct benchmark analysis on the 2014 two piece Jayhawk Motorsports wheel design. In this study, the hoop portions of the wheel are assigned composite material properties to match the currently manufactured laminate for these wheels. The materials used for the layup of this particular wheel are Park E765 T300 6K 5HS cloth and Park E765 T700 24K unidirectional tape, and the stacking sequence for the shell is as follows: [+/- 45, 0/90, 0, 0, 0/90]$_s$. The maximum displacement results for this wheel are listed in Table 5.4 below.

Table 5.4: JMS14 LC-4 displacements

Max Displacement Magnitude	0.109 in.
Max Displacement: longitudinal	0.052 in.
Max Displacement: lateral	-0.061 in.
Max Displacement: vertical	0.091 in.

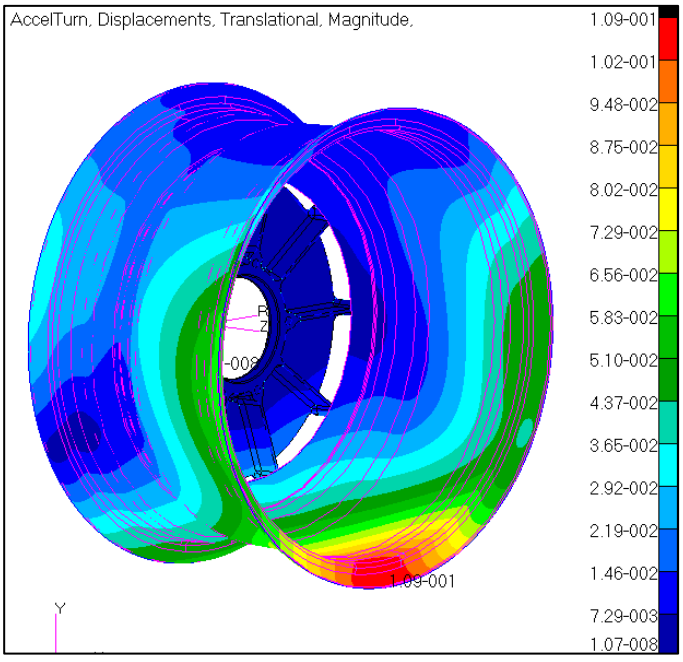

Figure 5.6: JMS14 wheel displacement

5.3 New Composite 5-Spoke Wheel Analysis

5.3.1 Preliminary laminate development

To develop a new preliminary laminate for use in the 5-spoke rim design, several laminate stacking sequence and material options are simulated in FEA. The wheel geometry, loading conditions and model setup used are the same as those of the JMS14 two piece composite wheel benchmark analysis. The results summary of this study are recorded in Table 5.5, which most importantly shows the resulting weight and maximum displacement magnitude in the rim for each laminate option. Based on these results, laminate number 7 was ultimately chosen for use in the new wheel. It provided one of the smallest displacements and lowest weights while maintaining full length plies (9-11 have shortened plies included).

Table 5.5: Laminate weight & displacement study

#	Nominal stacking seq.	Materials	Weight (lbs)	Max Displacement (in)
1	[±45, 0/90, 0, 0, 0/90]s	Park 6K 5HS, Park 24K uni	2.874	0.11
2	[±45, 0, 0, 0/90]s	Park 6K 5HS, Park 24K uni	2.374	0.126
3	[±45, 0/90, 0, 0, 0/90]s	Park 6K 5HS, Gurit HMC uni	3.306	0.0897
4	[±45, 90, 0, 0, 0/90, 0]s	Park 6K 5HS, Gurit HMC uni	3.57	0.079
5	[±45, 0/90, 0, 0, 0/90]s	Park 3K PW, Gurit HMC uni	2.778	0.113
6	[±45, 90, 0, 0, 0/90, 0]s	Park 3K PW, Gurit HMC uni	3.045	0.873
7	***[±45, 0, 0/90, 0, 0]s***	***Park 3K PW, Gurit HMC uni***	***2.505***	***0.112***
8	[±45, 0, 0/90, 0, 0]s	Park 3K PW (±45), Park 6K 5HS (0/90), Gurit HMC uni	2.834	0.1
9	[±45, 0b, 0, 0, 0/90]s	Park 3K PW, Gurit HMC uni	2.267	0.12
10	[±45, 0b, 0, 0/90, 0]s	Park 3K PW, Gurit HMC uni	2.267	0.119
11	[±45, 0, 0/90, 0b, 0]s	Park 3K PW, Gurit HMC uni	2.267	0.118

*b refers to a short ply covering bead area only

5.3.2 FEA model setup

General FEA model setup for the 5-spoke is similar to the benchmarking cases. The carbon fiber section of the wheel is modeled as a shell while the aluminum center insert remains a solid. QUAD4 shell elements are used to mesh the shell, with characteristic element size of 0.08” in the hoop, .04” in the spokes/center region and higher mesh density within high stress zones or areas of concern. The solid center is meshed with TET4 solid elements, characteristic size of 0.15” and refined in tight radii and contact zones. Glued contact zones were defined where the aluminum piece is bonded to the carbon rim; at the inner flanges faces and inside back face.

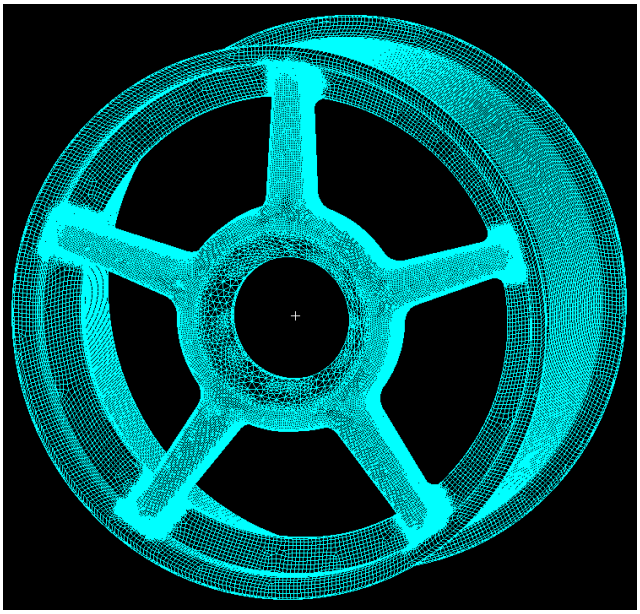

Figure 5.7: 5-spoke FE mesh

Aluminum 6061-T6 material properties are used for the solid center insert, and the composite shell is given the properties of laminate 7 as described in the previous section. Additionally, to more closely match the final manufactured wheel prototype, overlap of layers is included in the laminate at the radii transitioning from the spokes

to the hoop region. When modeling composite laminates it is critical that ply orientations are carefully considered and controlled in the FEA model. In this case, the composite shells are broken up into two main entities; the hoop and the spokes. While both share the same nominal laminate and stacking sequence, their laminate ply orientations do differ. In the hoop, the 0° plies are oriented along the circumference, so that the unidirectional material fibers basically create a continuous loop in order to better distribute the stresses. On the other hand, the spokes have the 0° plies oriented longitudinally, or axially, along each spoke since these members are predominantly under axial tension and compression and longitudinal bending.

The previously described load cases are applied to this model. Constraints are applied to the angled inner and outer faces and the drive pin holes on the aluminum center to represent the hub and nut assembly. Internal pressure is applied to the inside faces of the hoop. Vertical and lateral loads are applied to the same prescribed load application areas as before, and longitudinal load is again applied through a remote point attached to entire bead profile surface via RBE3 MPCs. As was the case in the benchmarking analysis, load case 4 (Table 5.1) provides the most extreme results so it is the primary concern of this study.

Details of the FE model setup and execution are provided in Appendix C.

5.3.3 Displacement results

After running the simulation, the first set of results observed are the displacements or deflections experienced by the model in order to compare against the benchmark analysis and determine if stiffness goals are met. As demonstrated in

Table 5.6, the deflection in the new 5-spoke design is less than that of the Keizer aluminum rim under the same load case. So, the current laminate for the 5-spoke rim meets the target goal by having higher stiffness by 19 percent. That being said, in order for the new design to be successful, it must also meet the prescribed strength goal and this is investigated in the following sections.

Table 5.6: Comparison of wheel LC-4 displacements

Max Displ.	5-spoke	Aluminum	JMS14
Magnitude	0.113 in.	0.140 in.	0.109 in.
Longitudinal	0.054 in.	0.061 in.	0.052 in.
Lateral	-0.065 in.	-0.087 in.	-0.061 in.
Vertical	0.092 in.	0.109 in.	0.091 in.

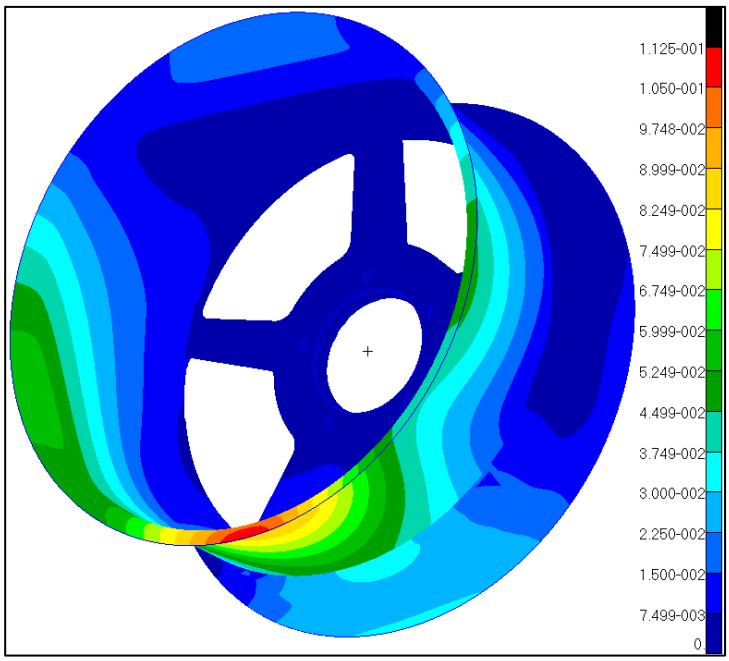

Figure 5.8: 5-spoke displacement magnitude

5.3.4 Composite failure criteria

Although achieving the target performance goals of reducing weight while maintaining acceptable stiffness is one major goal of the benchmarking analysis

study, the new wheel's structural integrity is of the utmost importance as well. This section describes how Patran/Nastran FEA software is used to analyze stress results in the rim model and measure against various failure criteria in order to explore the strength and safety of the new design. In order to check the composite laminate against failure, various commonly used composite strength failure criteria are investigated in Patran/Nastran. These include maximum strength, Hoffman, and Tsai-Wu theories. Each theory has a different formulation and unique characteristics, so they are compared in this thesis to determine which, if any in particular, provide a more acceptable means of analyzing failure for the composite wheel.

The most straight-forward of the failure criteria is maximum stress. Under the maximum stress failure criterion, each of the normal stress components in the principal material coordinates and the in-plane shear stresses must be independently less than the material's respective strengths in order to pass. Otherwise, the material is assumed to have failed with respect to the material's X_t, X_c, Y_t, Y_c, or S as defined below. It is important to note that that there is no interaction between the different modes of failure. Additionally, the stresses in the composite must be transformed to stresses acting in the principal material coordinates. Axis 1 is aligned with the principal fiber direction, axis 2 is perpendicular to axis 1 in the plane of the lamina and axis 3 is normal to both axis 1 and 2. This criterion is explained by the relationships below [6].

For tensile stresses: $\sigma_1 < X_t$, $\sigma_2 < Y_t$ *(5.1)*

For compressive stresses: $\sigma_1 > X_c$, $\sigma_2 > Y_c$ *(5.2)*

For shear stress: $|\tau_{12}| < S$ *(5.3)*

Figure 5.9 plots the experimental tension and compression strengths of a glass-epoxy composite against the maximum failure criterion with respect to varying orientation angles. As can be seen, the maximum stress criterion (shown as the solid curves) doesn't accurately represent the experimental data. In general, this criterion is not conservative for cases that are not dominated by just one component of stress [7].

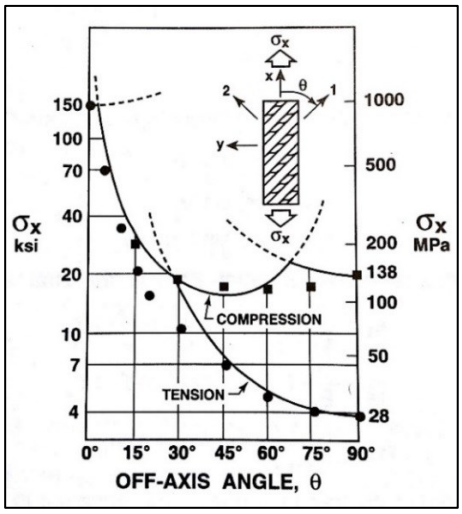

Figure 5.9: Maximum stress failure criterion [6]

The next consideration is the Hoffman's failure criterion. In this criterion, Hoffman modified Hill's yield criterion for orthotropic materials. In order to compare and more easily explain Hoffman, a brief description of the Tsai-Hill criterion should be provided. Tsai-Hill is an extension of the von Mises yield criterion for orthotropic materials. This leads to a single criterion as opposed to Maximum Stress, which has three. A shortcoming of Tsai-Hill is that it does not allow consider differing compression and tension material strengths. The governing equation for Tsai-Hill is as follows [6].

$$\frac{\sigma_1^2}{X^2} - \frac{\sigma_1\sigma_2}{X^2} + \frac{\sigma_2^2}{Y^2} + \frac{\tau_{12}^2}{S^2} = 1 \qquad (5.4)$$

Hoffman, similar to Tsai-Hill, develops a single failure criterion to test against the material's directional strengths. An advantage of the Hoffman failure criterion over Tsai-Hill is that it can account for different strengths in tension and compression. For cases considering plane stress in the 1-2 plane and material transverse isotropy in the 2-3 plane, the Hoffman failure criterion formulation is described by Equation 5.5 [6].

$$-\frac{\sigma_1^2}{X_cX_t} + \frac{\sigma_1\sigma_2}{X_cX_t} - \frac{\sigma_2^2}{Y_cY_t} + \frac{X_c+X_t}{X_cX_t}\sigma_1 + \frac{Y_c+Y_t}{Y_cY_t}\sigma_2 + \frac{\tau_{12}^2}{S_{12}^2} = 1 \qquad (5.5)$$

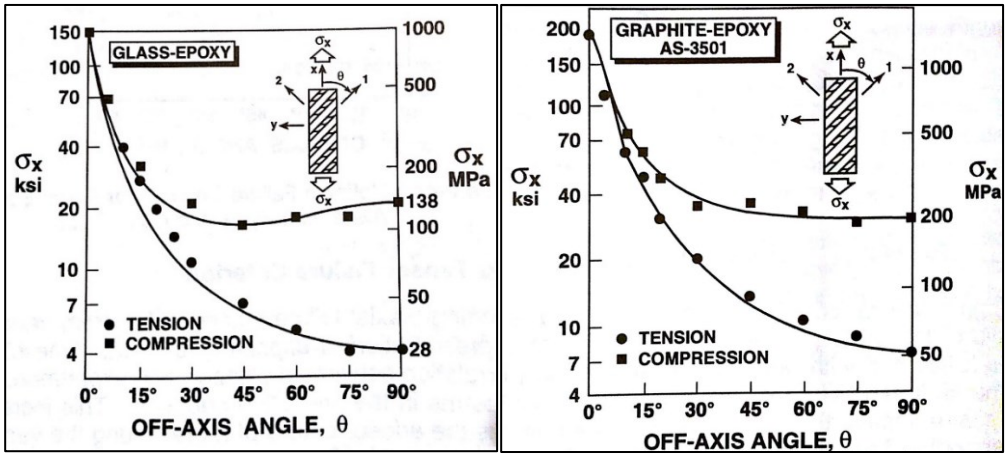

Figure 5.10: Hoffman failure criterion [6]

According to Jones [6], the Hoffman failure criterion offers some attractive attributes; the interaction between failure modes is considered, a single failure criterion is used for both in-plane tensile and compressive stresses, and for design use it is perhaps the simplest of the failure criteria. The plots in Figure 5.10 show a comparison between the Hoffman criterion and experimental failure data for glass-

epoxy and graphite-epoxy. The Hoffman criterion is in very good agreement with the test data, making it an apparently suitable failure criterion for these materials.

The Tsai-Wu tensor failure criterion was developed with more terms in order to improve its agreement with experimental data. In its original form, the criterion suggests that a failure surface exists in six-dimensional stress space, and if restricted to the case of an orthotropic lamina in plane stress, the general equation of Tsai-Wu failure is as follows [6].

$$F_1\sigma_1 + F_2\sigma_2 + F_6\sigma_6 + F_{11}\sigma_1^2 + F_{22}\sigma_2^2 + F_{66}\sigma_6^2 + 2F_{12}\sigma_1\sigma_2 = 1 \quad \textit{(5.6)}$$

Where:

$$F_1 = \frac{1}{X_t} + \frac{1}{X_c}\,,\; F_{11} = -\frac{1}{X_t X_c} \qquad \textit{(5.7)}$$

$$F_2 = \frac{1}{Y_t} + \frac{1}{Y_c}\,,\; F_{22} = -\frac{1}{Y_t Y_c} \qquad \textit{(5.8)}$$

$$F_6 = 0\,,\; F_{66} = \frac{1}{S^2} \qquad \textit{(5.9)}$$

$$F_{12} = \frac{1}{2\sigma^2}\left[1 - \left[\frac{1}{X_t} + \frac{1}{X_c} + \frac{1}{Y_t} + \frac{1}{Y_c}\right]\sigma + \left[\frac{1}{X_t X_c} + \frac{1}{Y_t Y_c}\right]\sigma^2\right] \qquad \textit{(5.10)}$$

The criterion's formulation ultimately makes it a more general case than Hoffman. Some of its advantages include invariance under rotation of coordinates and symmetry properties similar to the stiffnesses and compliances. Above all, the Tsai-Wu criterion theoretically has improved curve-fitting capabilities over the previously described criteria [6]. The Tsai-Wu failure criterion introduces a new coefficient, F_{12}. This coefficient depends on the material's strengths and tensile failure stress, σ, and is obtained from a biaxial test. It should be noted, however, that

the biaxial test required for F_{12} determination is expensive and difficult to conduct. As can be seen in Figure 5.11, it seems that the F_{12} has relatively small influence on the failure surface. For these reasons, Narayanaswami and Adelman suggest that F_{12} may simply be considered to be zero [6]. Figure 5.12 gives a basic comparison between some of the failure criteria. The presented plots illustrate that the results of each of the failure criteria can vary, so it is important to understand or determine which criterion best fits the needs of the design. This can be a function of the specific material in question and test result correlation, as well as FEA capabilities and computational efficiency if applicable.

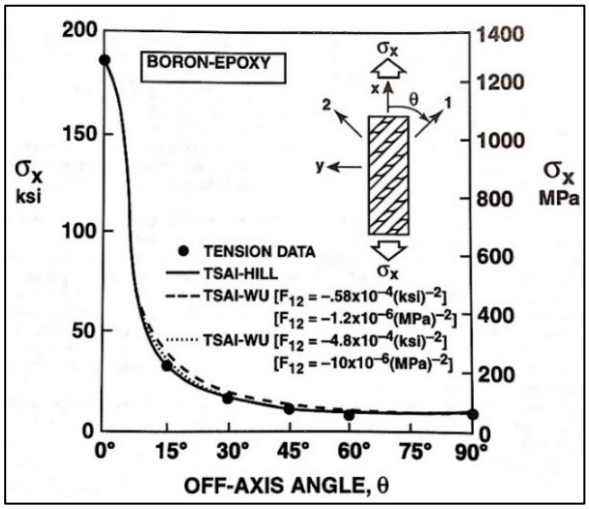

Figure 5.11: Tsai-Wu tensor failure criterion [6]

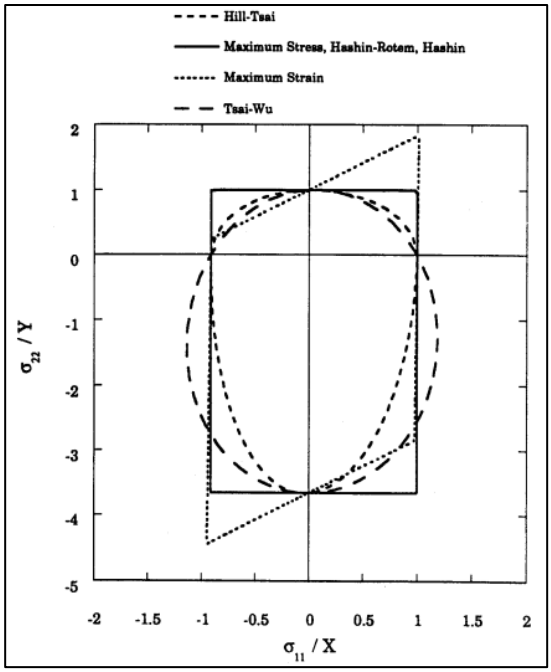

Figure 5.12: Comparison of failure criteria [26]

5.3.5 Strength and failure analysis

Through the use of MSC Patran and its Laminate Modeler tool for post processing, results for the previously mentioned failure criteria are evaluated. The results are then compared to determine whether any of the criteria are better suited than the others for failure evaluation of the wheel design under investigation. As was done previously, only the most extreme scenario, load case 4, will be discussed in detail here. Additional results and information from all load cases can be found in the appendix. After the Nastran analysis is run and the results file is attached in Patran, the Laminate Modeler tool is used to calculate results for the selected failure criteria. The program does this by extracting the stress tensor results from the structural analysis and combining those with material strength limits as specified in the previously discussed failure criteria. There are a number of composite failure options

that can be chosen including reserve factors, failure indices, margins of safety, and critical components.

To begin the composite failure evaluation, the reserve factor (RF) results for each lamina are plotted. The reserve factor can also be considered as the safety factor, where an RF equal to 1 means material is at failure, so the two are synonymous as used within this thesis. The lowest reserve factor is observed for each criterion. These reserve factors are compared against each other to determine if there are any significant differences. In this study, there is slight variation amongst the results for these three different failure criteria. Of the three, Hoffman provides the most conservative reserve factor and it is considered to be the simplest for use in design according to Jones [6], so it is selected as the failure criterion of choice for this study.

Table 5.7: Worst reserve factors

Failure Criterion	Worst Reserve Factor
Maximum Stress	1.62
Hoffman	1.53
Tsai-Wu	1.54

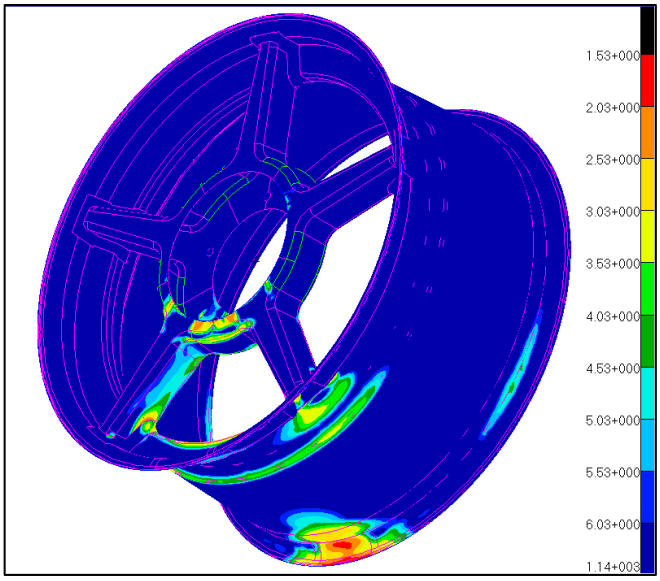

Figure 5.13: Worst Hoffman reserve factors

Since the results are similar for each criterion, the area with the lowest factor of safety, is easily determined – it is shown in red in the Figure 5.13 plot in the lower portion of the inner hoop. Through investigation of the reserve factors for each layer, it is determined that the layer with ply ID 1009 is the most critical layer. This layer has the lowest reserve factor of 1.53, which represents first ply failure. Now, it is not only important to determine which ply or zone will fail first, but also to determine the potential failure mode in this region. A ply can experience either matrix failure or fiber failure. Laminates are usually fiber strength driven, so a matrix failure would not necessarily mean complete or catastrophic failure of the component, although it would degrade transverse and/or shear properties of the specific ply, therefore quite possibly impacting the component's behavior or performance and potentially decreasing its overall strength. In order to determine which failure mode is most likely to occur, the stress tensors' components are plotted and compared. The stress

tensor components are evaluated in material orientation coordinates; the X component refers to σ_1, Y refers to σ_2, and so on. Strength ratios (R) are calculated for each component using the Equation 5.11. The lowest maximum stress strength ratio will designate the failure mode.

$$R = \frac{\sigma_{ultimate}}{\sigma_{applied}} \qquad (5.11)$$

This procedure is used on the determined critical ply, 1009, which is the second to last layer going around the circumference of the rim hoop in the model. As shown in Table 5.8, the lowest strength ratio is produced by the X component, or 1 direction, of stress in compression. This ply is a unidirectional lamina, so this means compressive fiber failure.

Table 5.8: Layer 1009 strength ratios for LC-4

Tensor Component	Material Component	Ultimate Strength (ksi)	Applied Stress (ksi)	Strength Ratio
X_t	σ_{1t}	226.5	26.48	8.55
X_c	σ_{1c}	122.3	76.68	1.59
Y_t	σ_{2t}	4.17	2.34	1.78
Y_c	σ_{2c}	12.05	0.93	12.96
XY	τ_{12}	9.38	1.80	5.21
YZ	τ_{23}	9.38	0.67	14.00
ZX	τ_{13}	9.38	1.15	8.16

From Figure 5.13, it is observed that there are also a couple high stress concentration points along the bottom edge of the center hole where the aluminum insert is bonded. It should be noted that these high peak stresses are likely to be artifacts of geometry and contact conditions. This assumption is based on the observation that the stresses along the edge are not distributed uniformly, instead the

peak stress seems to occur in one or two points which would not be the case for this round feature. The surrounding areas in the spokes generally show significantly larger reserve factors, and in the spokes laminate, the worst reserve factor is about 2 at the edge between the bottom spoke and the hoop, near the low RF spot for layer 1009.

For comparison, the lowest Hoffman reserve factors results from each load case are listed in Table 5.9 below. This confirms that load case 4 is the most extreme loading scenario and results in the lowest reserve factor, or safety factor, in the wheel. With a minimum reserve factor of 1.53, the new 5-spoke composite wheel exceeds the strength of the baseline aluminum alternative. This also meets the general FAA (FAR) requirement of a 1.5 safety factor for structures [35] and 1.4 for composites [37].

Table 5.9: Lowest Hoffman reserve factors per load case

Load Case	Low Reserve Factor
1	5.68
2	4.56
3	1.56
4	1.53
5	2.10
6	6.57

Table 5.10: Comparison of aluminum and 5-spoke wheel safety factors

5-Spoke CF wheel min. safety factor	Aluminum wheel von Mises safety factor (yield)	Difference
1.53	1.23	24%

5.3.6 Fiber misalignment study

Since the composite materials being used are considered orthotropic, variation in ply or fiber misalignment can lead to undesired or under-performing structural characteristics in the manufactured part. For this reason, it is important that fiber misalignment be kept to a minimum, or at least be controlled within a determined tolerance. This is especially the case for components that are laid up by hand, such as this wheel, where there is a higher likelihood in ply misalignment if care is not taken. It is good practice to establish a control tolerance of fiber misalignment for manufacturing in order to reduce the risk of unwanted behavior or premature failure during operation of the product. With that in mind, the effects of fiber misalignment is studied for the design of the new five spoke composite wheel in order to develop a general fiber misalignment tolerance for manufacturing.

For this study, the same FE model is considered, but the laminate's ply orientation reference angles are adjusted globally. The analysis is done in two steps; first, the plies are offset by 5° and then by 10°. As before, displacement and strength results are observed and recorded in the following table.

Table 5.11: Ply Misalignment Results

Ply misalignment	Max displacement	Min reserve factor
0°	0.113”	1.53
5°	0.115”	1.51
10°	0.123”	1.41

The results from this study show that there is only a slight degradation in stiffness and strength with 5° of misalignment in all plies. For 10° of ply misalignment,

the stiffness and reserve factor are almost 9% and 8% lower, respectively. In terms of stiffness, the result of the 10° misalignment is still acceptable since the displacement remains smaller than that of the aluminum wheel. In order to maintain a minimum safety factor of 1.5, it is recommended to control global ply misalignment to 5° or less.

5.4 Analysis Discussion

Overall, the analysis has shown that composite laminate developed for the 5-spoke wheel design does meet and exceed the original performance goals. The new lightweight rim is 19% stiffer than the baseline aluminum alternative which will lead to a lower amount of dynamic camber change due to wheel compliance. In terms of strength, the analysis shows that the wheel will not fail and that its ultimate strength design safety factor is 11% higher than the aluminum wheel. The minimum reserve factor is 1.53 in a localized region which is deemed acceptable for such a structure. From the ply misalignment study, it was also determined that global ply misalignment should not exceed 5° in order to maintain a safety factor above 1.5, and this guideline may be used as a future layup tolerance. Since this study only considers uniform global misalignment, future work could consider investigating worst case scenarios with compounded ply misalignment as well.

A majority of the rim shows very high safety factors so it is possible that thinner laminate stacks can be used in some areas to lighten the wheel even more, but care must be taken not to reduce the overall stiffness or strength too much. Additionally, it is possible that amounts of misalignment greater than 5° may be tolerable in the lower stress areas of the laminate without decreasing the minimum safety factor.

Investigation of more advanced and nonlinear failure theories can also be considered for additional comparison to those employed in this thesis. Investigation of progressive ply failure may also be considered in future work for additional insight to failure characteristics.

It should be noted that the limit load cases applied to the rim represent maximum tire forces from ideal track and tire conditions, meaning that the tires will likely not experience such high forces for sustained periods of duration. Those tire contact patch loads are then applied directly on to the rim surface, making the model conservative since some force absorption and distribution by the tire is neglected.

Of course, there a number of ways the analysis can be performed with higher detail – such as including a correct tire model, modeling the adhesive rather than using a glued contact, meshing the composites with fine 3D solid shell elements, and using a multi-component assembly to more accurately fixture the wheel. However, such methods can greatly increase the complexity and time required to successfully simulate wheel behavior.

6 Manufacturing

This chapter discusses the methods and processes practiced for the manufacturing of the composite rim developed within this thesis.

6.1 Molds and Tooling

6.1.1 Aluminum molds

As mentioned in chapter three, it was decided to repurpose an old wheel design and therefore utilize its previously manufactured aluminum tools. Of course, the large aluminum molds need modifications in order to meet the requirements for the redesigned wheel center geometry. To make these changes, a simple modular tool design approach is used. First of all, the 4-lug bosses in the center spoke faces are machined flat since they are no longer needed in the wheel. Three additional round aluminum pieces are machined and bolted to the large molds in order to create surfaces on which to layup and create the desired geometry. One piece is a thin disk with chamfered edges that is bolted to the center inside face of the mold that creates the mating chamfer between the wheel center and the hub. Another disk with matching inside chamfer, that basically mimics the inside end of the center insert, is machined and will be used to sandwich the composite skin between it and the inside face to create a flat bonding surface. The third piece is a disc with longer sides that is

bolted to the center outside face and will be laid upon to create the circumferential bonding tabs. The following figures show the aluminum tooling to be used for the composite layup.

Figure 6.1: Aluminum tooling

As shown in Figure 6.1, the aluminum tooling provides female mold surfaces for the spokes and male mold surfaces for the rim hoops. Because there are two main pieces that are bolted together, the layup occurs in two basic steps and will be described in section 6.2.3. To describe briefly, however, the prepreg CFRP laminae are laid up directly onto these aluminum mold surfaces.

It should also be noted that the original molds were completely solid aluminum, making them very heavy and likely leading to slow and non-uniform heating during the curing cycle. In order to resolve these issues, a large section of the inner mold is machined on the backside making it lighter, but still maintaining sufficient structural integrity, to improve the heat transfer and distribution while curing.

6.1.2 Trapped rubber tooling

Perhaps the most interesting aspect of the tooling stems from the special needs of creating the hollow spokes. Like most manufacturing problems, there are a number of possible solutions and for this case a few options were briefly outlined in the background section. For this particular design, the goal is to create completely hollow spokes with no permanently trapped tooling or core, and so it was decided to utilize removable and reusable rubber tooling as a male insert for the hollow spoke portion of the rim. There are several options and suppliers for this type of rubber and because JMS has a close relationship with Airtech International, their Aircast 3700 RTV high temperature casting compound was ultimately chosen. One of the benefits of this specific material is that it has a large coefficient of thermal expansion as compared to aluminum meaning that it will apply high pressure to the laminate during elevated temperature curing, something that is necessary since this internal region will not see pressure from vacuum bagging or the autoclave. Additionally, Aircast 3700 has a relatively high strength and flexibility, making it a good choice as a reusable tool [27].

Generally speaking, the tooling process is quite similar to that used by Blackstone to manufacture CFRP racing motorcycle wheels [12]. The basic procedure for manufacturing the rubber tooling is as follows: create female mold to match the desired finished interior spoke dimensions and release, prepare and mix the two-part rubber per manufacturer's instructions, pour the mixture into the molds and cure at elevated temperature as required. After the rubber cures, it is removed from its mold as a single piece and then cut into several pieces to aid in the future

removal process. Images depicting the rubber tooling are shown below. The idea is that after laying up the CFRP onto the aluminum molds, the rubber pieces will be placed in the uncured spokes prior to tool assembly, followed by curing. Upon cure completion and demolding from aluminum, the trapped rubber tooling is removed from the CFRP rim, leaving clean and hollow spokes.

Figure 6.2: RTV rubber tooling

6.2 Composite Manufacturing Process

There are several steps involved in the manufacturing of a laminated composite structure, and those taken for the manufacture of the CFRP 5-spoke rim are outlined in this section.

6.2.1 Lamina preparation

Prior to layup, the prepreg CFRP laminae must be prepared and this occurs in a couple of steps. First, because the material being used is prepreg that is stored in a frozen state to maintain proper resin performance, it must be thawed and allowed to

warm up to room temperature which can take a couple of hours. Once the material has reached room temperature, it is ready to be cut into plies of predetermined shapes. Ideally, ply templates are created using ply development software and then cut on automatic CNC ply cutting tables, but due to resource limitations both these steps are done by hand in the JMS lab. Ply templates are shaped and cut by hand using heavy paper so they may be marked on and reused. In the end several different templates are created for the different regions of the wheel such as the inner and outer hoops, spokes, and bond tabs. After templates are developed, then plies are cut in necessary quantities and orientations corresponding to the previously determined stacking sequence. Basic equipment for cutting the plies includes scissors, utility blades, ruler, and right angle. It is also important to ensure that the environment in which the material is being cut and all equipment is cleaned and free of contaminants – acetone or denatured alcohol can be used for this.

6.2.2 Tooling preparation

The next major step that must occur prior to layup is the preparation of the molds or tools. First it is important that the mold surfaces, in this case the aluminum, are smooth and polished in order to ease the demolding process and also to obtain a nice, glossy finish on the final part. Next it is necessary to clean and degrease the tools carefully, again using a solvent such as acetone or denatured alcohol, in order to prevent exposure of the CFRP to contaminants that could negatively impact the curing or matrix performance. Once cleaned, the tools must be properly released to ensure successful demolding after cure. To do this, releasing agent is applied to the mold surface prior to layup. Two release agents are used for this particular project;

Loctite Frekote solvent based release and Airtech Safelease water based PTFE release. The Frekote is applied to aluminum tooling and the Safelease to the rubber, following provided manufacturer's instructions. After having been sufficiently released, the aluminum molds are preheated in the oven to about 100°F to help the first layer of prepreg stick to the mold and therefore allow for better handling and more accurate layup.

6.2.3 Layup

The general layup process for the composite rim is done in a conventional manner for prepreg laminates, following the previously determined 10-layer stacking sequence from chapter five. Ultimately, the wheel is laid up in two parts; first both the inner and outer portions are partially laid up separately and then they are put together and the remainder of the material is laid to join them into a single composite piece. In the first step, all ten layers of the spokes are applied but only the first five layers are laid on the hoop portion. The spoke plies on the outer portion of the tool have about an extra 0.25 inches of length on the edges to provide sufficient overlap onto both the outer hoop area and the inner portion of the spokes. Layers in the spoke and hoop sections are alternated so that the ply overlaps are intertwined. The 5-layer bonding tabs are laid up and positioned after the spokes areas are done. After the two separate halves of the tooling are laid up, they are debulked under vacuum at room temperature for several hours. Next, a piece of peel-ply is laid over the center inside skin to provide a good bonding surface. The peel-ply used is a thin fiberglass cloth coated in PTFE that is laid onto the laminate surface, and when removed after cure leaves a matte and nicely textured surface that is good for

adhesive bonding. Then the rubber spoke tools are inserted into the deeper, outer section of the mold on top of the laminate, and the extended edges are folded over for overlap prior to setting the inner portion on top and bolting everything together tightly. Once the two halves are fastened together, the remaining five hoop layers are applied in a manner ensuring sufficient overlap between inner and outer side plies to allow for secure joining of both parts. At the end, additional layers of a thicker CFRP material, a Park E765 12k woven fabric, are applied only to the tire bead area and function as sacrificial layers that provide enough thickness for the machining of the designed bead hump profile.

Figure 6.3: Partial layup of inside mold

Once the laminate layup is complete, the part is vacuum bagged and debulked prior to curing. Commonly practiced bagging procedures are used with the following materials from Airtech, in order from the part surface out: Wrightlon perforated release film, Airweave breather cloth, and Wrightlon bagging film.

6.2.4 Curing

After the bagged, uncured part has debulked for a few hours, it is ready to be cured. A final cure temperature dwell of 240°F for 4 hours, as mentioned in chapter 3, with ramp rates of 4°F/min is chosen for the given materials. The part is cured using this cure cycle in the JMS autoclave with a pressure of 50 psi. While the CFRP manufacturers state that their materials can be oven-cured under vacuum alone, the decision was made to utilize the autoclave with elevated pressure in order to get better surface finish and laminate compaction. Upon completion of cure cycle, the wheel is left to cool down before the bagging material is removed, tools are disassembled, and the cured rim is carefully demolded.

6.3 Aluminum Center Manufacturing

Figure 6.4: Aluminum center machining

In addition to complete and careful manufacturing of the composite rim, this thesis project also requires the in-house manufacturing of the aluminum center insert

that was described and shown in the design chapter. Being a single piece of aluminum, the insert is machined at the JMS shop on their 3-axis Mazak CNC machining center. The programming and simple fixtures were developed to allow for use of currently stocked tools and vice to hold the part during machining. Programming was done through the use of HSMWorks cam software. A simple two-fixture process was developed for the machining – starting with a rectangular bar held in the vice, the back side features are machined first with undersized drive pin holes that are then threaded, then the part is flipped over and fastened to a plate to hold it down for the machining of the outside, center hole, and angled nut face. Fine finishing passes are used so that little to no sanding or polishing is required on the nut surface. After machining, the drive pin holes are drilled out to the correct 0.25" diameter, and the part is complete.

6.4 Final Processing

Upon completion of the layup and aluminum insert machining, there are two remaining manufacturing steps to finish the wheel.

6.4.1 Rim machining

The CFRP rim requires machining to finalize its geometry, which is again performed on the JMS CNC machine with the rim being positioned and clamped onto the machine table using its aluminum mold as a secure fixture. From the manual layup, the outermost rim edges are extra-long and uneven, so these are milled to match the design model. The tire bead profiles are then machined around the hoop

using a continuous rim diamond coated circular blade with fine tool paths to avoid the need for final sanding or polishing. Finally, the five drive pin holes are drilled into the inside skin of the rim.

Figure 6.5: Machined bead profile

6.4.2 Bonding process

The final step in manufacturing is the assembly and bonding of the CFRP rim and aluminum insert. Before any epoxy resin is applied, careful surface preparation must be performed. First, the bonding surfaces of the CFRP tabs and the aluminum insert are lightly sanded with medium to fine grit sand paper or emery cloth to create a slightly roughened surface that will assist with adhesion. The inner center face of the rim does not need to be sanded since it already has a favorable surface finish from the peel ply. After sanding, all dust and debris must be completely removed and then the surfaces are thoroughly cleaned and degreased using a solvent such as denatured alcohol. Although it is not done for the prototype due to time and resource constraints, it is also recommended practice to treat the aluminum for corrosion resistance prior to bonding since the untreated, direct carbon-to-aluminum interface could lead to galvanic corrosion over time. Common and effective treatments include Alodine coating or anodizing of the aluminum, and this has to be done after all

machining and sanding/abrading. After the parts have been carefully cleaned, they are then set aside to dry completely, and care must be taken to avoid any further contamination. The parts should be bonded soon in order to ensure they are still clean, if left out for a long period of time they should be cleaned and degreased again prior to application of adhesive.

A readily available two-part epoxy adhesive, Hysol 9309.3NA, was chosen for this project. Besides already being stocked in the JMS lab, this epoxy was chosen for its high strength and because it contains small glass beads that provide good bondline thickness control. Prior to bonding, the epoxy is mixed per the manufacturer's instructions [38] and then carefully applied to the aluminum bonding surfaces. Temporary pins through the drive pin holes are used to align and guide the aluminum insert into its final position. Once in place, excess epoxy is wiped away and the assembly is placed in the oven. Weights are carefully placed on top of the aluminum to apply pressure, and the adhesive is cured at 180°F for one hour. Once cured and the wheel has cooled, the new 5-spoke composite rim is complete.

The final weight of the finished 5-spoke prototype is 3.17 lbs. The extra 0.17 lbs compared to the model weight is likely due to the extra bead area layers, the epoxy to bond in the aluminum insert and the resulting overlaps from layup.

Figure 6.6: Complete rim prototype

7 Prototype Testing

While the FEA simulations provide promising results for the expected success and performance of the 5-spoke composite wheels, it is recommended that physical testing of a prototype be conducted for validation. There are several standardized testing procedures that automotive wheel manufacturers must subject their designs to in order to receive certification for safe use on public roads, however these tests require high-end equipment and facilities currently not available to the JMS team. The required tests for certification include basic strength, impact strength, and fatigue/cyclic strength in various loading scenarios that can represent extreme or accidental circumstances seen in reality on a full-sized road car. While these kinds of tests are necessary for wheels on production vehicles, the FSAE race cars operate in much more ideal circumstances where impact and high long-life scenarios are not present. So, for the purpose of this thesis, two simple in-house tests are performed on a manufactured prototype rim and the results are described in this chapter.

7.1 Compression Load vs. Displacement Test

In this case, a structural test is conducted in Patran/Nastran and replicated physically using the ME department's MTS machine for verification. The test performed is a simple compression test where load and displacement are measured.

The rim is placed in the MTS machine with the inner edge of the rim supported on a plate, and then a compressive, vertical load is applied to the outside center of the rim. A dial indicator is used to measure the displacement of the center insert throughout the test and the test setup is shown in the figure below.

Figure 7.1: Rim displacement test setup

In addition to the physical testing performed, an FEA model is developed to simulate the test. Results from both are compared to see if the physical and simulation test results correlate. A compressive load up to 400 pounds is applied to the rim center. The maximum displacement measured in the physical test is 0.0085 inches and the FEA shows a displacement of 0.0075 inches, a 13% difference. While this is not a perfect match in displacement, the correlation between the slope of the test and simulation lines is very close at higher loads. This indicates that there may

have been some compliance or settling in the test rig and setup at the start of loading. That in mind, the results are still relatively close especially considering the small scale of the deflection being measured by a dial indicator and possible variations in physical material properties. A comparison and correlation of the current results is presented in Figure 7.2.

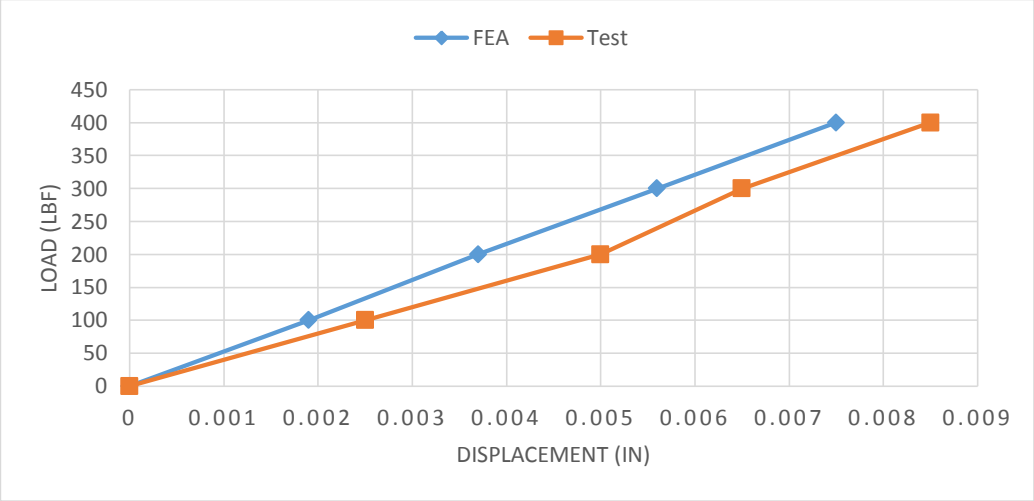

Figure 7.2: Comparison of FEA and compression load test results

Higher fidelity static testing, as well as dynamic test may be considered in the future for further FEA validation efforts.

7.2 Operating Temperature Test

Like most materials, laminated composites have a safe operating temperature limit and if it is exceeded, its performance and structural integrity are significantly impacted. For epoxy resins, this elevated temperature limit is called the glass transition temperature (T_g). If the temperature rises above the material's T_g range, the epoxy matrix transforms from a rigid or "glassy" state to a more pliable or "rubbery"

state [28], which could lead to failure of the structure. The T_g varies depending on the specific epoxy matrix and the cure temperature is generally the limit, so it is important to stay well below that temperature. A good rule of thumb is to remain 50° F under.

Due to the nature of the wheel's operating conditions, there are sources of heat generation during operation of the vehicle that could potentially affect the rim. Heat could be transferred through the tire from friction on the road surface, and, perhaps more significantly, the heat from the brakes could also be transferred to the rim either by radiation or by conduction through the wheel hub. For this reason, it is necessary to determine whether the temperature of the composite rim could exceed the temperature of 240°F used for curing of the Hysol epoxy adhesive.

To do this, a simple test was conducted by placing temperature indicating labels in different locations on CFRP wheels and driving the car for extended periods of time, similar to what may be experienced in an endurance race – the case in which the brakes would get the hottest. The strips used have range from 104-160°F with ten points that will turn black if the corresponding temperature is reached and their placement can be seen in the following images. Three trials of driving the car for an extended period of time with heavy brake use, recreating conditions of an endurance race each time, were run in an ambient temperature of about 80°F. After conducting the trials, the wheel was removed to see the results on the strips. The first point of strips on the carbon fiber rim were activated, meaning that the rim only reached between 104-108°F, as shown in Figure 7.3. Additional testing at higher ambient temperature may be beneficial to consider racing on a hot summer day, but the

temperature gain recorded here is well enough below the glass transition temperature and recommended threshold that it is not likely to be of concern.

Figure 7.3: Temperature indicating strips on rim

8 Conclusion

Through the design, analysis, and manufacturing efforts carried out in this thesis project, a lightweight single piece composite rim prototype has been successfully developed for use on the JMS FSAE racecars and other similar racing environments. The 5-spoke rim exceeds the goal of maintaining the stiffness of a commercial aluminum option while significantly reducing the weight and maintaining structural integrity. As designed for the specific load cases studied herein, the 5-spoke rim provides almost 19% higher stiffness than the popular Keizer aluminum wheel and at 3.17 lbs, the manufactured prototype is 60% lighter. The weight loss in the wheels alone can benefit the FSAE cars' acceleration and handling by reducing rotational, unsprung mass as well as decreasing the yawing moment of inertia by 7%. This will lead to a more agile and responsive racecar, especially if additional vehicle weight loss strategies are employed.

Even though the wheel is so light, FEA results show that sufficient strength is maintained with no apparent failure under the extreme load cases applied and a minimum safety factor of 1.53. Simple physical tests were performed to validate both the FEA displacement results as well as material mechanical properties with reasonable correlation. Of course with additional time and resources, further wheel testing would be of benefit. This could include modal testing for additional verification of the FE model stiffness as well as SAE standardized wheel testing.

The manner in which the FEA model was created allows for its efficient use on computers that are currently available to the JMS team. It provides for a comprehensive yet uncomplicated analysis of the 5-spoke single piece composite wheel that can serve as a good basis for further development and investigation for potential future JMS design efforts.

Additionally, an efficient composite rim manufacturing process, new to the JMS team, was successfully developed. The multi-step process including re-useable rubber tooling and a bonded center insert is easily implemented using the team's readily available resources and facilities.

Utilizing the information provided by this thesis as a basis for further composite wheel development and use, the JMS team can not only improve the driving performance of their racecars but also advance their state of the art in composite structures production.

References

1. Society of Automotive Engineers (SAE), "Rules Formula SAE", 2014.
2. Hoosier Tires, “Collegiate Formula SAE”, 2015. <www.hoosiertire.com/Fsaeinfo.htm>
3. The Tire and Rim Association, Inc. (TRA), “J (ISO) Contour Standard”, 2007.
4. W. F. Milliken and D. L. Milliken, Race car vehicle dynamics vol. 400: Society of Automotive Engineers, 1995.
5. Carroll Smith, Tune to Win: The Art and Science of Race Car Development and Tuning: Carroll Smith, 1978
6. Robert M. Jones, Mechanics of Composite Materials 2nd Edition: Taylor & Francis, 1999.
7. Ever J. Barbero, Introduction to Composite Materials Design: Taylor & Francis, 1999.
8. SAE, “SAE Vehicle Fixed Coordinate System”
9. L. Eckstein, Längsdynamik von Kraftfahrzeugen: Verkehrssystem Kraftfahrzeug, Kräfte am Fahrzeug, Antriebstrang, Bremsen, Fahrleistungen und Verbrauch; Vorlesungsumdruck Fahrzeugtechnik I: Forschungsges. Kraftfahrwesen, 2014.
10. E. M. Kasprzak and D. Gentz, "The Formula SAE Tire Test Consortium-Tire Testing and Data Handling," 2006.
11. Hexcel, “HexPly Prepreg Technology”, 2013.
12. Alan Cathcart, “Blackstone TEK/BST Factory: Black Gold”, Sport Rider Magazine, 2011. <www.sportrider.com/sportbikes/blackstone-tek-bst-factory-black-gold>
13. J. Tomblin, J. McKenna, Y. Ng and K. S. Raju, “B-Basis Design Allowables for Epoxy-Based Prpreg: FiberCote Graphite Fabric T300 3KPW / E765”, NIAR AGATE-WP3.3-033051-103, 2001.
14. J. Tomblin, J. McKenna, Y. Ng and K. S. Raju, “B-Basis Design Allowables for Epoxy-Based Prpreg: FiberCote Graphite Fabric T300 6K 5HS / E765”, NIAR, Rep. 02-2 rev. 1, 2003.
15. J. Tomblin, J. McKenna, Y. Ng and K. S. Raju, “B-Basis Design Allowables for Epoxy-Based Prpreg: FiberCote Graphite Unitape T700 24K / E765”, NIAR, AGATE-WP3.3-033051-104 rev. 1, 2004.
16. Garry Jolliffe, Gurit, “Design Properties for SE70 HMC300”, e-mail correspondence, Apr. 2015.
17. David L. Harris, “Modeling of fracture and durability of paste-bonded composite joints subjected to hygro-thermal-mechanical loading”, Master’s thesis, Missouri University of Science and Technology, 2013.

18. D. Hull and T.W. Clyne, An Introduction to composite Materials 2nd edition: Cambridge University Press, 1996.

19. ASTM Standard D3039, “Standard Test method for Tensile Properties of Polymer Matrix Composite Materials”, ASTM International, 2014.

20. ASTM Standard D2344, “Standard Test Method for Short-Beam Strength of Polymer Matrix Composite Materials and Their Laminates”, ASTM International, 2013.

21. Gurit, “SE 70 Low Temperature Cure High Toughness Epoxy Prepreg System”, general datasheet, 2015.

22. Park Electrochemical Corp, “E-765 Epoxy Prepregs”, general datasheet, 2012.

23. S. Timoshenko and S. Woinowsky-Krieger, Theory of Plates and Shells Second Edition: McGraw-Hill, 1959.

24. K. Yay and I. Ereke, “Fatigue Strength of a Rim Model with FEM Using a New Approximation Technique”, SAE technical paper 2001-01-3339.

25. A. Rupp and A. Heinrietz, “Simulation of the Experimental Proof Out of Wheels and Hubs”, SAE technical paper 2002-01-1202.

26. C. Sun, B. Quinn, J. Tao and D. Oplinger, “Comparative Evaluation of Failure Analysis Methods for Composite Laminates”, DOT technical report DOT/FAA/AR-95/109, 1996.

27. Aircast International, “Aircast 3700: RTV high temperature casting compound”, technical datasheet, 2015.

28. Epoxy Technology, “T_g – Glass Transition Temperature for Epoxies”, 2012.

29. MSC Software, “Patran 2014 User’s Guide”, 2014.

30. MSC Software, “Patran 2014.1 Laminate Modeler User’s Guide”, 2014.

31. MSC Software, “NAS113 Online Training (Composite Material Analysis with MSC Nastran)”, 2014.

32. Koenigsegg, “Koenigsegg Reinvents the Wheel”, 2012. <www.koenigsegg.com/koenigsegg-reinvents-wheel>

33. C. Chamis, “Mechanics of Composite Materials: Past, Present, and Future”, Journal of Composites Technology & Research, JCTRER, Vol. 11, No. 1, Spring 1989, pp. 3-14

34. Voigt W. Uber die Beziehung zwischen den beiden Elastizitatskonstanten Isotroper Korper. Wied. Ann, 38 (1889) 573-587.

35. Code of Federal Regulations, “Title 14: Aeronautics and Space; Chapter 1: FAA DOT; Subchapter C: Aircraft, Part 25: Airworthiness Standards – Transport Category Airplanes; Subpart C: Structure; §25.303: Factor of Safety”, Amdt. 25-23, 35 FR 5627, 1970.

36. R. Hale, “Ultrasonic nondestructive evaluation techniques and the effects of fiber architecture on mechanical performance in multi-directionally reinforced textile composites, Appendix 3: Analytical Determination of Out-of-Plane Thermo-Elastic Properties for Laminated Composite Plates”, PhD Dissertation, Iowa State University Department of Aerospace Engineering and Engineering Mechanics, 1995.
37. FAA Commercial Space Transportation, “Guide to Verifying Safety-Critical Structures for Reusable Launch and Reentry Vehicles”, Version 1, November 2005.
38. Henkel Corporation, “Hysol EA 9309.NA: Epoxy Paste Adhesive” Rev. 10/99, technical datasheet.

APPENDIX

Appendix A: Insert Bond Area Calculation

A simple calculation was done to determine sufficient surface area for bonding the aluminum insert into the CFRP rim. The hand calculation is shown below. For simplicity and conservativeness, an extreme torsional load is considered that would not be experienced in real life. The case used assumes that the center insert is fixed only by circumferential bond area and that there is now CFRP laminate between the insert and the hub. The required minimum bond area calculated is greatly exceeded in the final design.

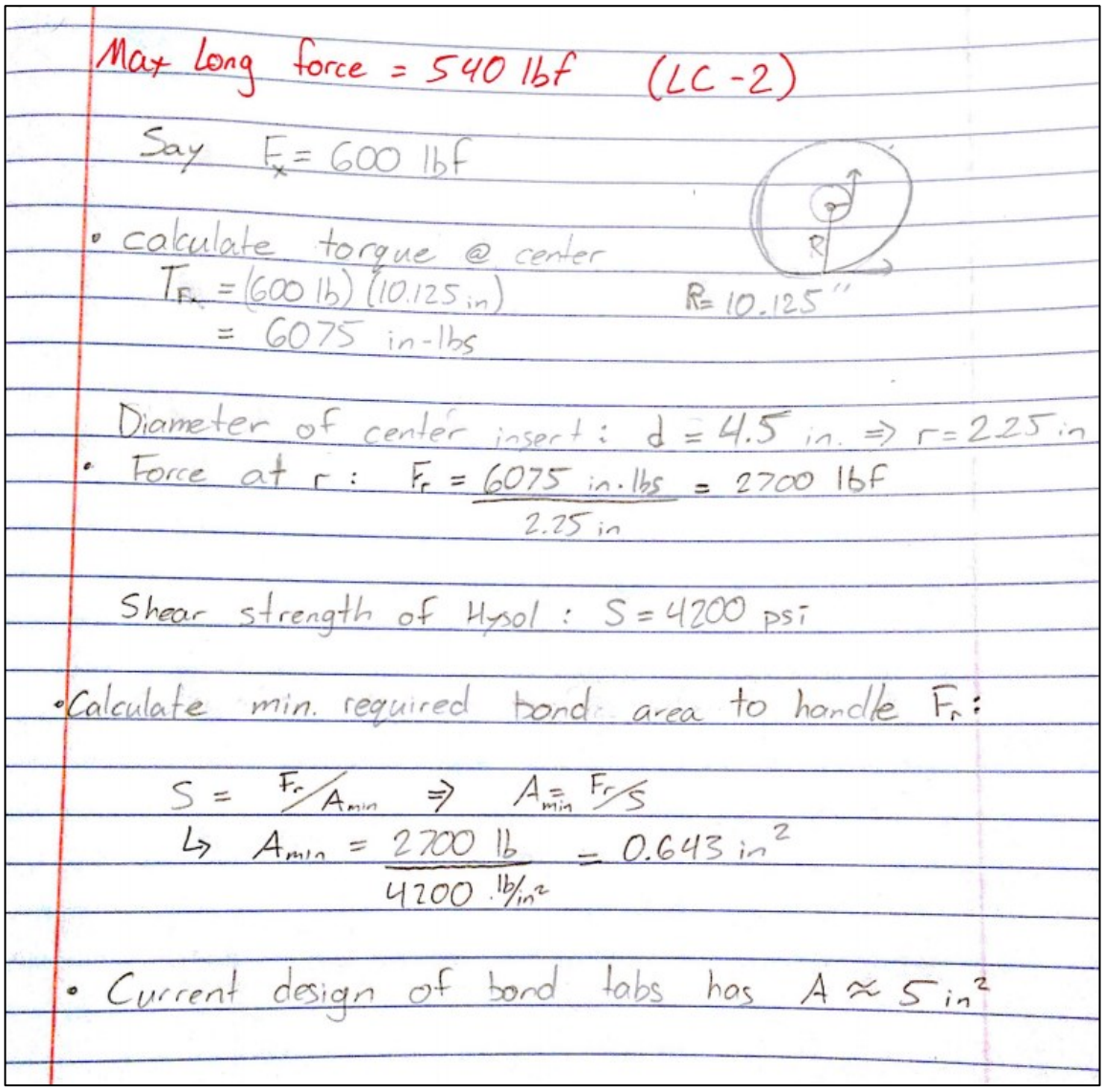

Appendix B: Aluminum Rim FEA Report

Title

Keizer 13" Aluminum Rim

Executive Summary

The results of this study are used to develop a baseline performance target for the new composite wheel design. Under the most extreme load case, the aluminum rim had a max displacement of 0.140" and a minimum ultimate safety factor of 1.23 in the spokes. The new design should give lower displacement and a higher safety factor.

Problem Statement

Structural analysis of the aluminum rim under most extreme load case (Max Acceleration + Turning). Deflection and strength results will be used as performance baseline for new wheel design.

System Properties

Component	Weight (lb)	Material
Center	2.1570	6061-T6
Inside Hoop	3.8970	6061-T6
Outside Hoop	1.5840	6061-T6
Total	7.6380	

Shell thickness = 0.125"

Material	E	ν	σ_{yield}	$\sigma_{ultimate}$
Al 6061-T6	10 Msi	0.330	40 ksi	45 ksi

Model Geometry [see figures in Geometry page]

Geometry of wheel assembly obtained from Keizer website as IGES file and imported to SolidWorks. Fasteners removed. Rim hoops converted to surfaces (center left as solid). Load application surfaces created on hoops. New assembly geometry saved as parasolid.

Parasolid file imported to Patran. Aluminum 6061 property applied to each component. Rim hoop shells and center fastened together via glued contact around bolting flanges (no fastener hardware included).

Mesh [see figures in Mesh page]

Component	Element Type	Method	Global Size (in)	# Elements
Center	TET10	TetMesh	0.1	389346
Inside Hoop	QUAD4	Paver	0.1	31105
Outside Hoop	QUAD4	Paver	0.1	13072

Total	433523

Notes:

TetMesh Param: Max h/L = 0.06 ; Min edge length = global edge length*0.01

Paver param: Max h/L = 0.06

Nodes equivalenced in each shell after paver meshing

Loads and Restraints [see figures in LR page(s)]

Only the most extreme load case is reported: max acceleration + turning. The three parts are "glued" together in the flange regions rather than modeling fasteners.

Loads

Load Type	Location	Magnitude	Direction	Notes
Pressure	Inside Surfaces of rim	10 psi	Normal	Common nominal operating tire pressure.
Force	Contact patch center	280 lbf	Longitudinal, Global X	Applied through MPC covering the tire bead area, simulating longitudinal (rotational) force on tire.
Total Load	Vertical load area on bead	380 lbf	Vertical/radial, global Y	Represents radial/vertical load on tire
Total Load	Lateral load area on inner bead	650 lbf	Lateral, -Z global	Represents lateral loading on tire

Restraints

Restraints	Location	Magnitude	Direction	Notes
Displacements	Center hub diameter	0	XY	Acts as hub constraint.
Displacements	Inside hub face and nut face	0	Z (Axial)	Acts as inside hub and nut constraint.
Glued Contact	Center flange to outside flange			Master: Center, Slave: outer rim
Glued Contact	Outside flange to inside flange			Master: Outside rim, Slave: inner rim

Analysis of Results [see figures in Results page(s)]

Component	Max Eq. Stress (von Mises)	FS (yield)	Max Deflection
Outer hoop	11.4 ksi	3.51	0.140”
Inner hoop	21.0 ksi	1.90	

Center	32.5 ksi	1.23	

Notes:

Stresses in rim shells mainly act like a loaded hoop/pipe

FS in center spoke is low

Outer hoop peak stress near bottom portion of bolting flange

Inner hoop peak stress in radius around outside edge in loading region

Center peak stress at radius edge of back side bottom spokes near the center circular portion

Conclusions/Recommendations

This study establishes the baseline performance target for the new composite rim design. The new design should have less than 0.146" of max displacement and at least a 1.2 (yield) factor of safety for the applied load case.

Even though the FS of the wheel center is quite low, the loads applied are extreme and likely not reached during normal operation of the FSAE car.

Geometry:

Original 3D CAD

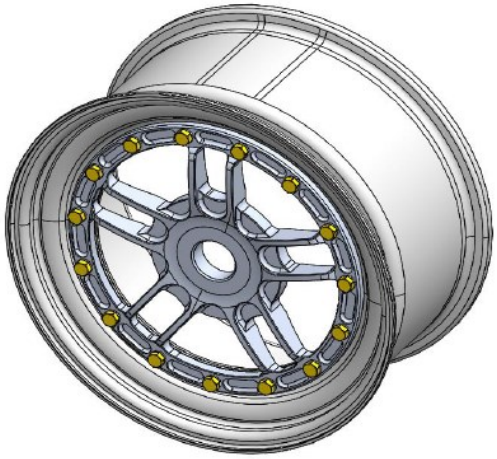

FEA CAD

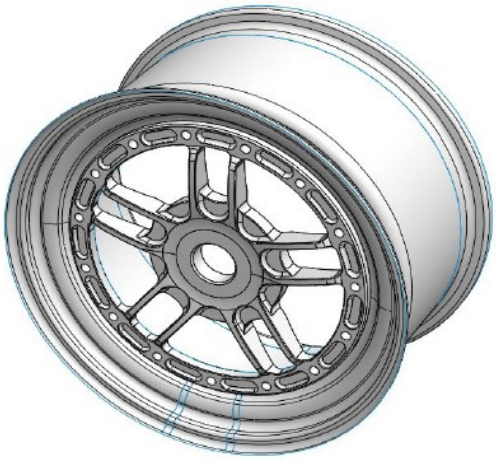

Geometry in Patran

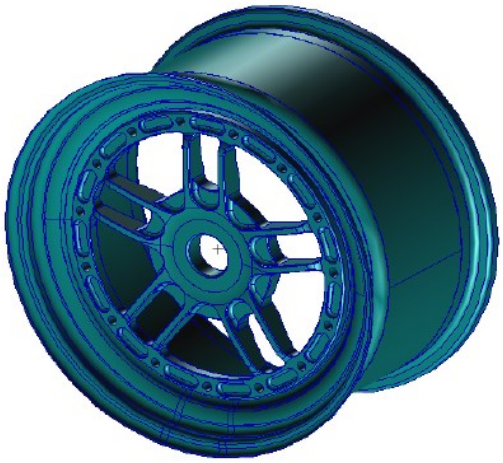

Mesh:

Global

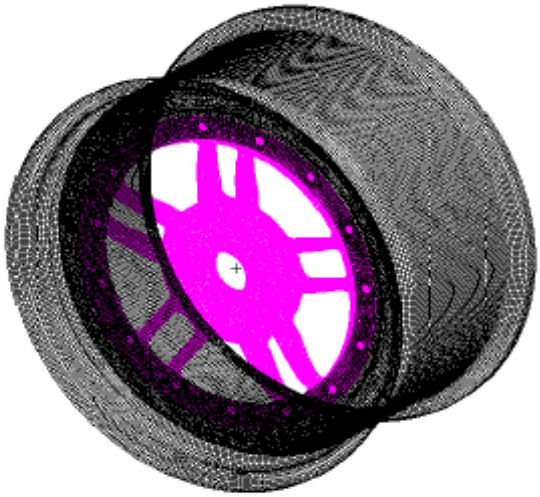

Center

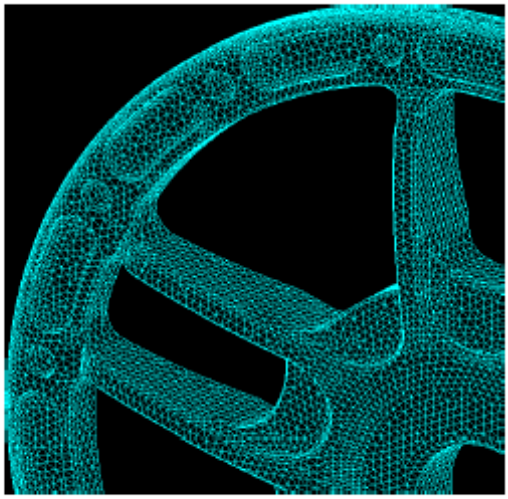

Outer Shell

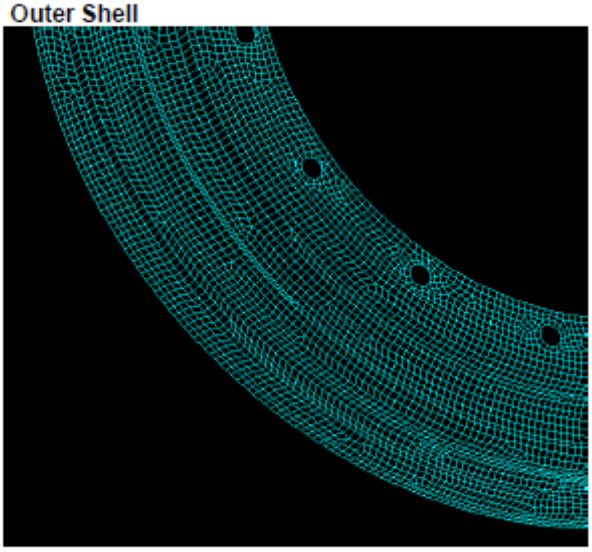

Inner Shell

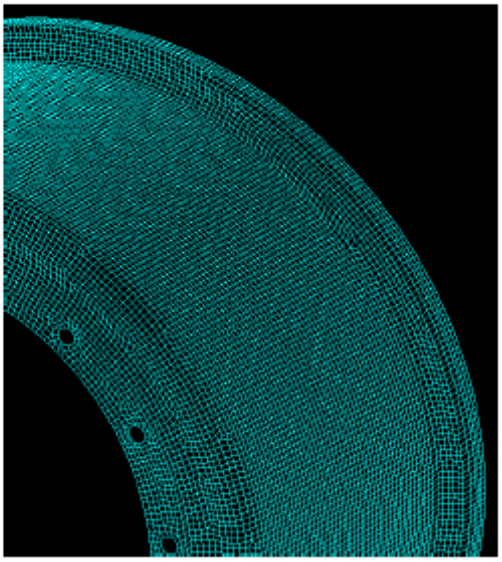

MPC

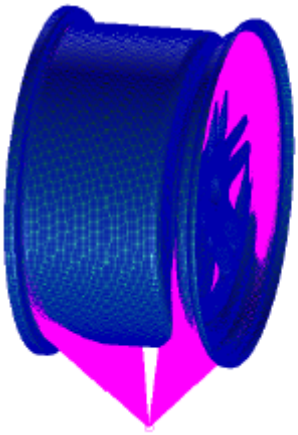

Loads & Boundary Conditions:

Constraints

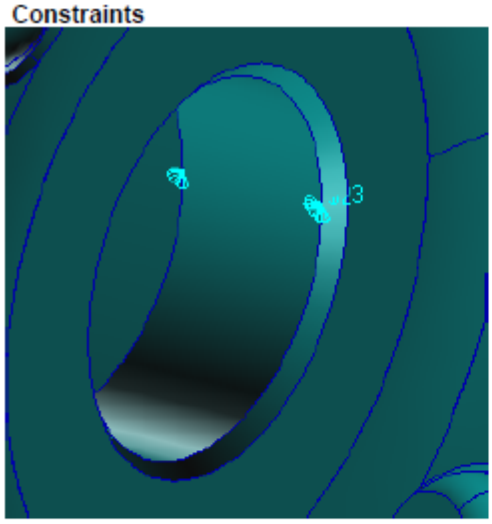

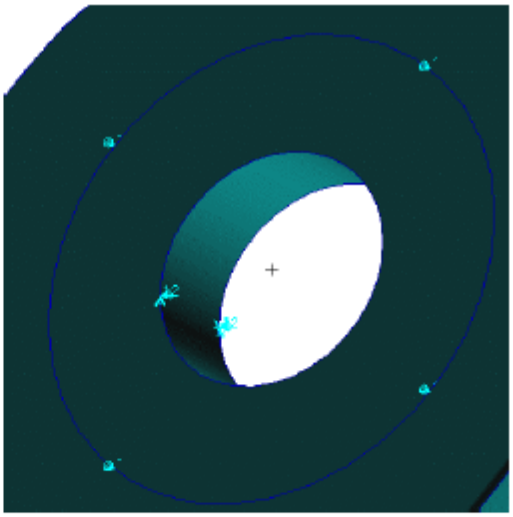

Radial Total Load

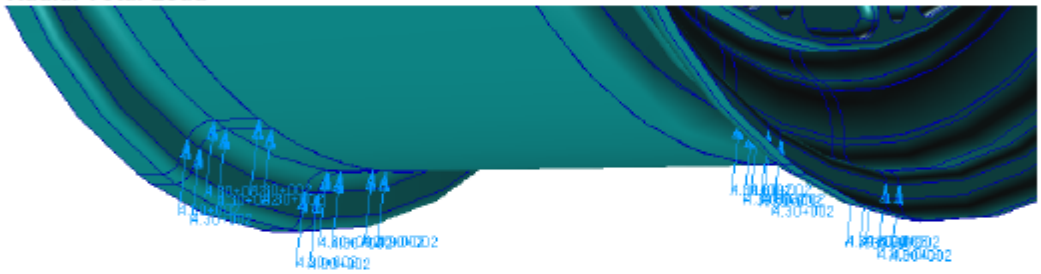

Lateral Total Load

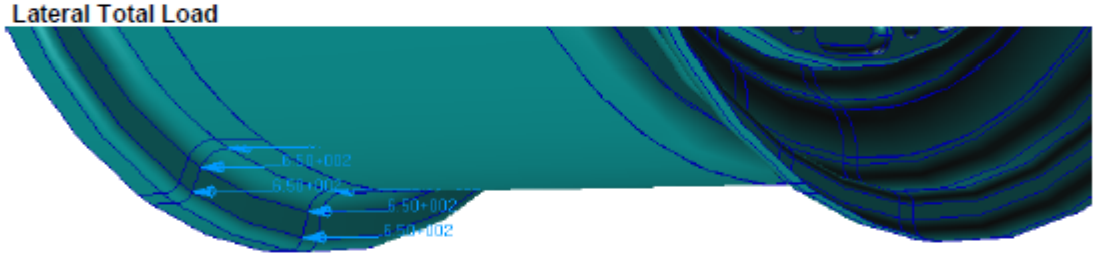

Longitudinal Force

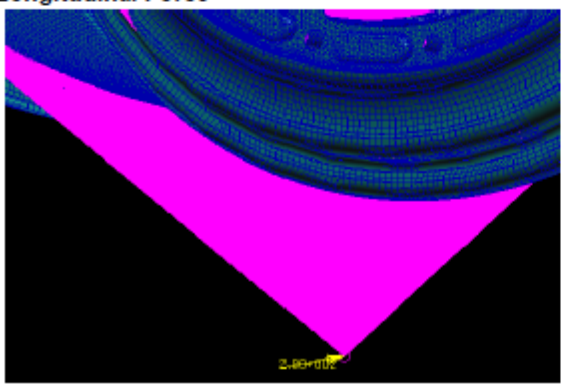

Pressure

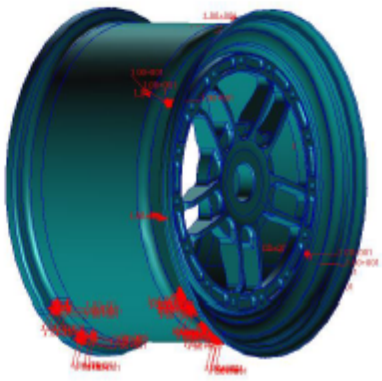

Result Plots:

Displacements (Magnitude)

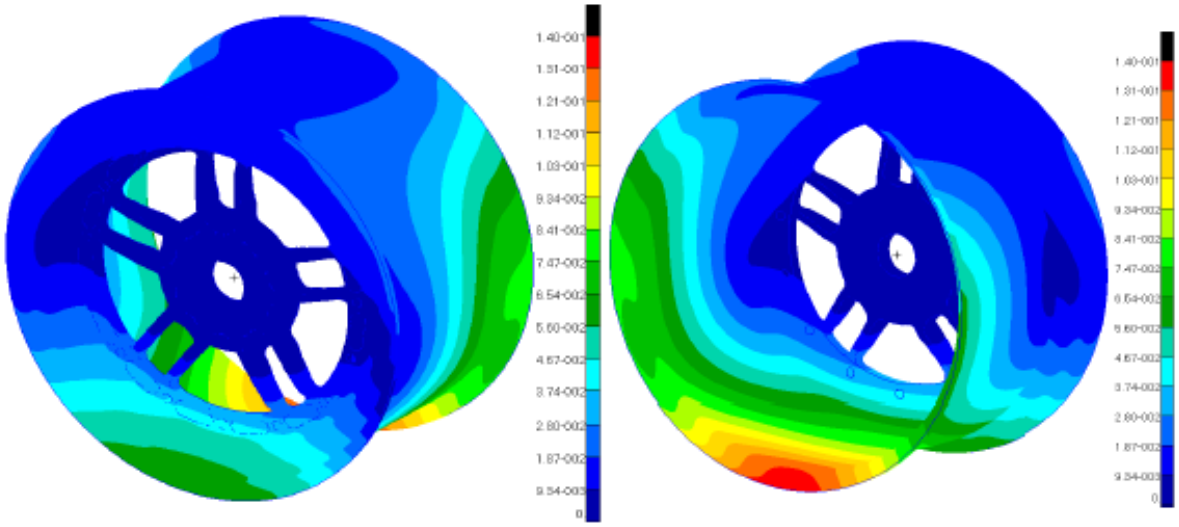

Eq Stress: Outer Shell Z1

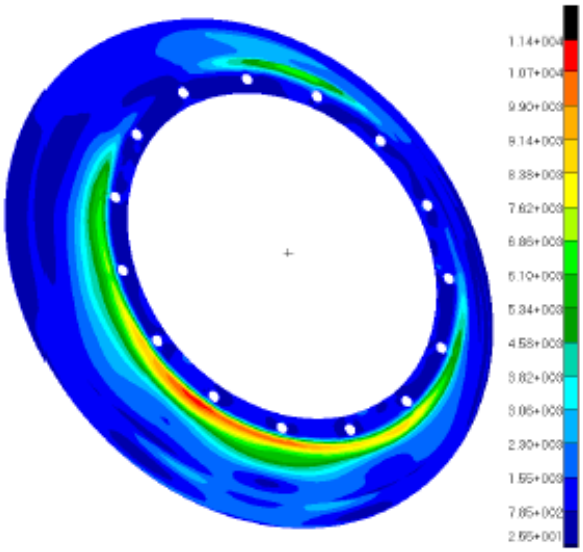

Eq Stress: Outer Shell Z2

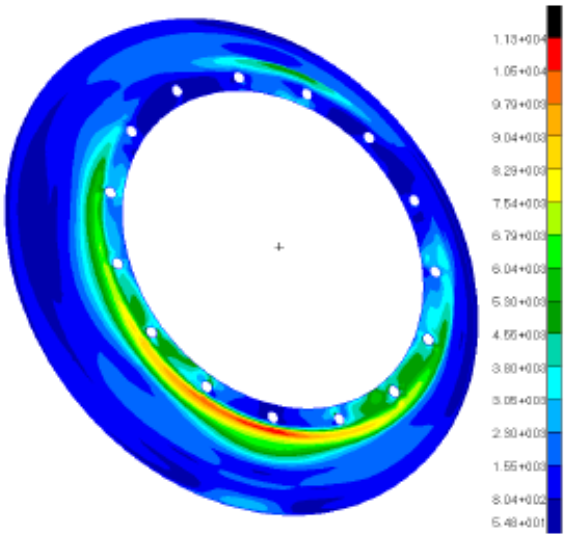

Eq Stress: Inner Shell Z1

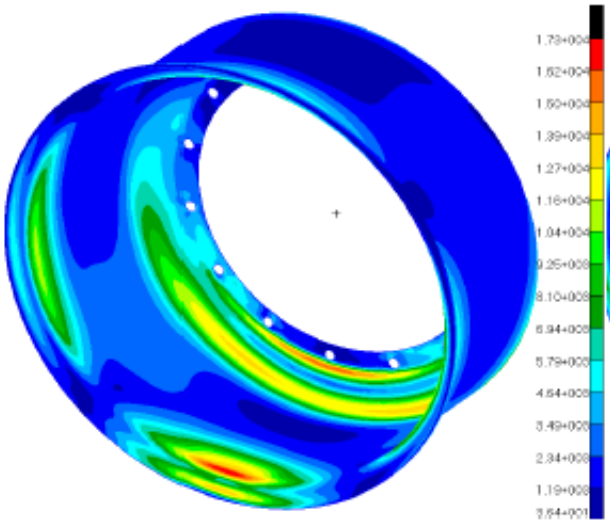

Eq Stress: Inner Shell Z2

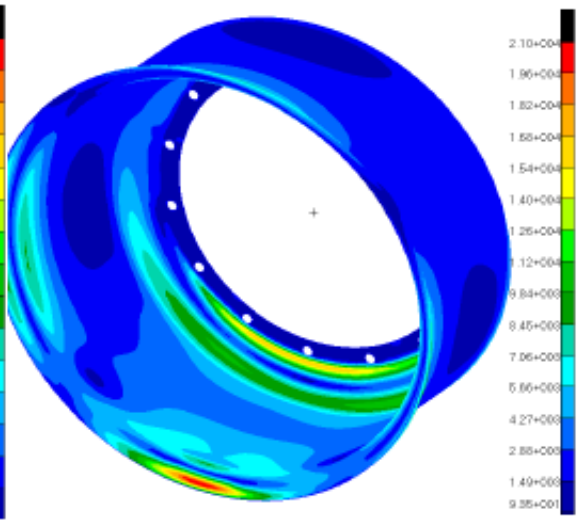

Eq Stress: Center

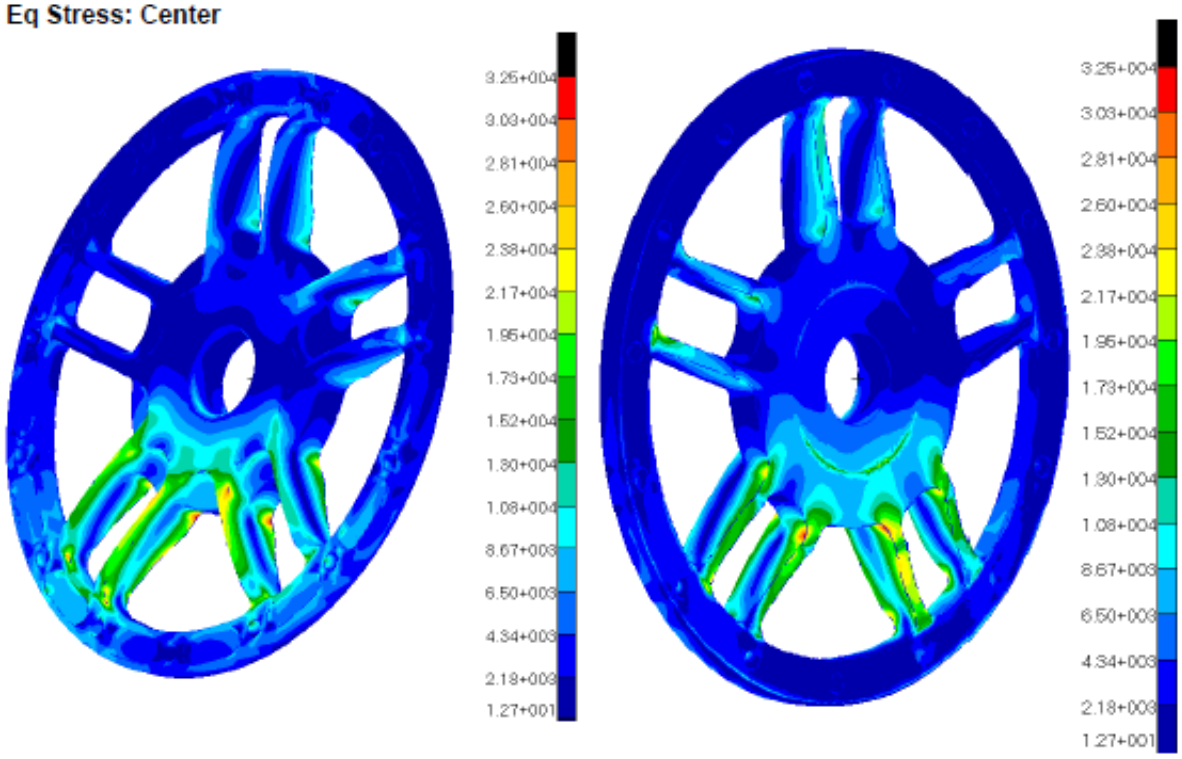

Appendix C: 5-Spoke CF Rim FEA Report

Title

13" 5 Spoke CF Wheel

Executive Summary

This study examines the performance of the 5 spoke composite wheel under the most extreme load case. With a maximum displacement magnitude of 0.113" and a safety factor of 1.53 (Hoffman RF), in addition to its low weight, it meets and exceeds the performance baseline established by the Keizer aluminum rim.

Problem Statement

Perform structural analysis of the newly designed 5 Spoke composite rim under most extreme load case (Max Acceleration + Turning). Deflection and strength results will be evaluated to determine if design meets previously established performance targets from aluminum study.

System Properties

Component	Weight (lb)	Material
Center	0.5046	6061-T6
CF Rim	2.4990	CF Laminate*
Total	3.0036	

* See material properties for Park E765/T300 3K PW and Gurit SE70/HMC300 uni in Chp. 4 and laminate stacking sequence in Chp. 5

** Laminate in spokes oriented at 0° aligned with global radial direction. Hoop oriented with circumferencial direction.

Model Geometry [see figures in Geometry page]

3D CAD model of wheel generated in SolidWorks. Composite rim is modeled as shell and aluminum center insert remains solid.

Parasolid file imported to Patran. Aluminum 6061 property applied to center insert. Shell is given laminate properties, as defined in Chp. 5. Laminate modeler tool used to create plies around hoop.

Mesh [see figures in Mesh page]

Component	Element Type	Method	Global Size (in)	# Elements
Center	TET4	TetMesh	0.15	49357
Rim Hoop	QUAD4	Paver	0.08	169099
Rim Spokes	QUAD4	Paver	0.04	
			Total	218456

Notes:

Meshing parameters: Max h/L = 0.06
Radii around end of spokes refined: size = 0.02"
Nodes equivalenced in after paver meshing

Loads and Restraints [see figures in LR page(s)]

Only the most extreme load case is reported: max acceleration + turning. The aluminum center and CF shell are fastened by "glued" contact.

Loads

Load Type	Location	Magnitude	Direction	Notes
Pressure	Inside Surfaces of rim	10 psi	Normal	Common nominal operating tire pressure.
Force	Contact patch center	280 lbf	Longitudinal, Global X	Applied through MPC covering the tire bead area, simulating longitudinal (rotational) force on tire.
Total Load	Vertical load area on bead	380 lbf	Vertical/radial, global Y	Represents radial/vertical load on tire
Total Load	Lateral load area on inner bead	650 lbf	Lateral, -Z global	Represents lateral loading on tire

Restraints

Restraints	Location	Magnitude	Direction	Notes
Displacements	Center hub diameter	0	XYZ	Acts as hub constraint.
Displacements	Drive Pin holes	0	XY	Acts as drive pins, constraining rotation.
Glued Contact	Center Al circumference to bonding tabs			Master: Center, Slave: CF bonding tabs
Glued Contact	Center Al back to inside rim face			Master: Center, Slave: inside rim face

Analysis of Results [see figures in Results page(s)]

Component	Min. Hoffman RF	Min. Tsai-Wu RF	Min. Max-stress RF	Max Deflect.
Shell Hoop	1.53	1.54	1.62	0.113"
Center	**Nom. Min FS (von Mises):** 3.33			

Notes:

Lowest RF in PLY ID 1009 at inside loading region. This is a uni ply and RF 1.53 is in axial compression.

There are exagerated peak stresses on the bottom edge of the center insert and shell hole feature due to artifact of geometry/glued boundary conditions.

Hoffman criterion provides most conservative reserve factor.

Conclusions/Recommendations

The results of this study show that the 5 spoke composite wheel does meet and exceed the baseline performance target. It has a higher factor of safety and lower deflection than the aluminum alternative.

Geometry:

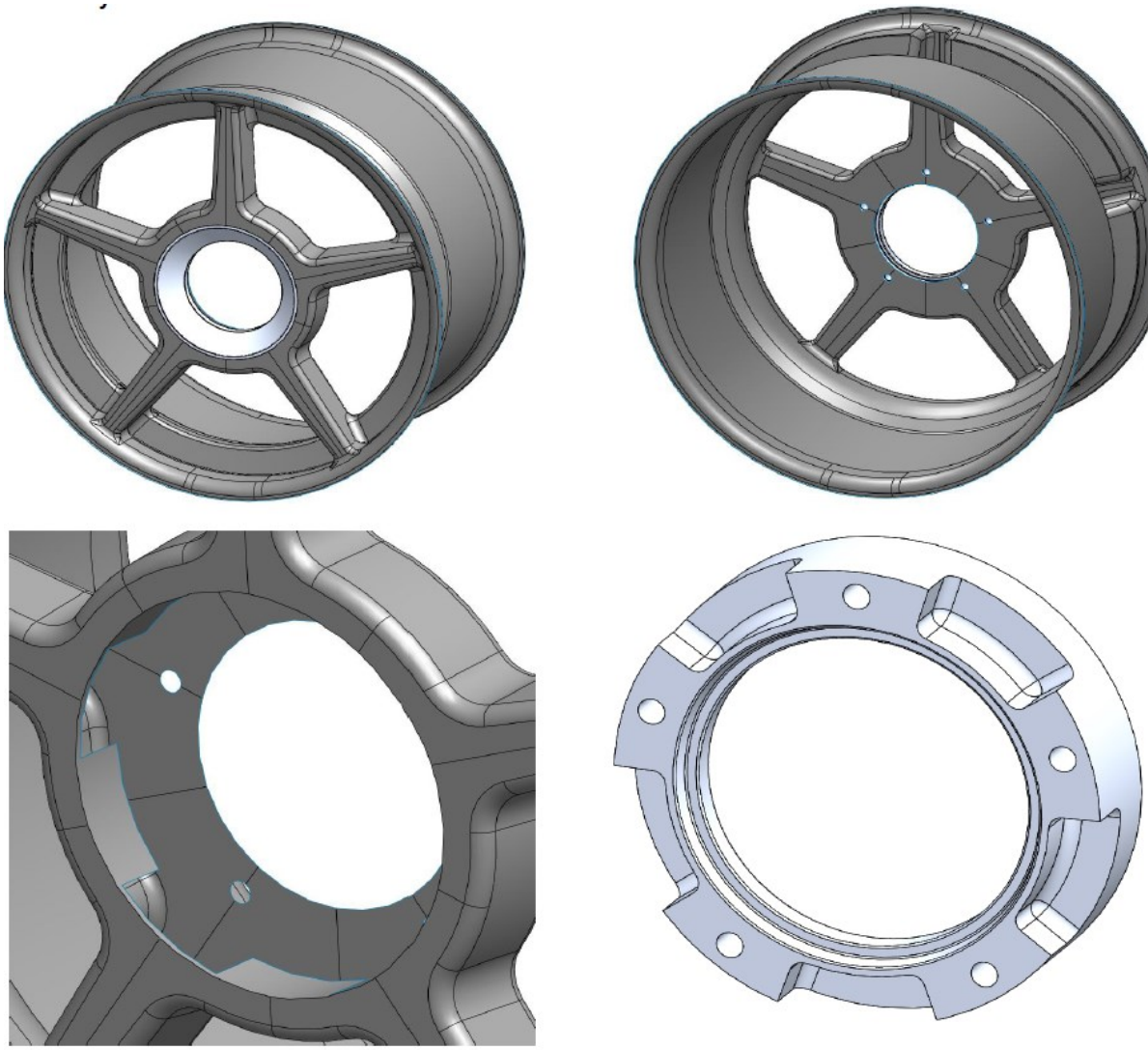

Mesh:

Global

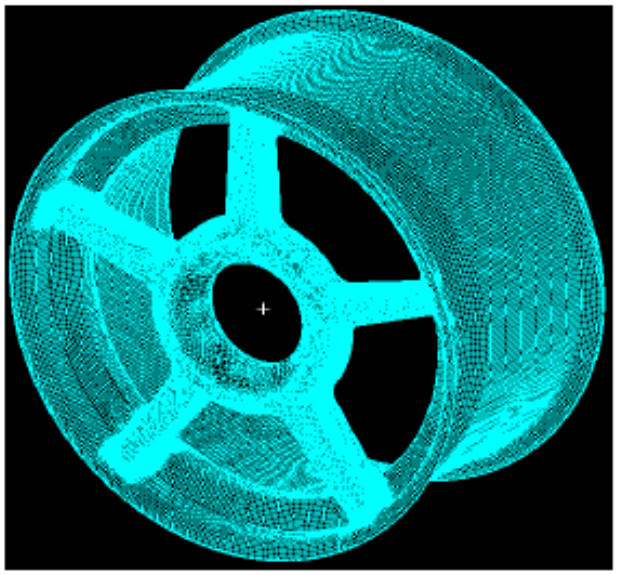

Center

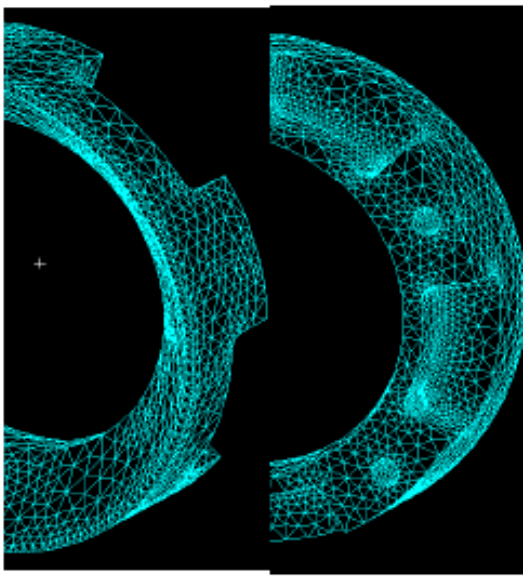

Shell

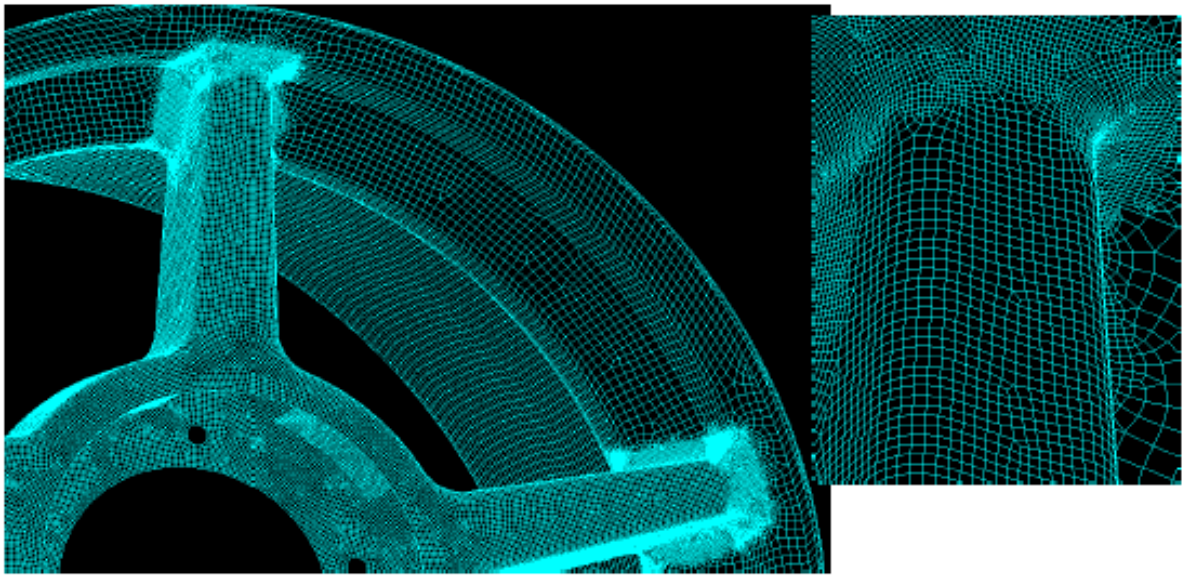

MPC

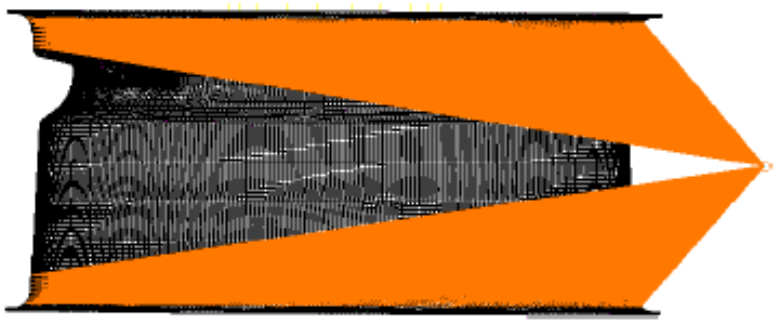

Loads & Boundary Conditions:

Constraints

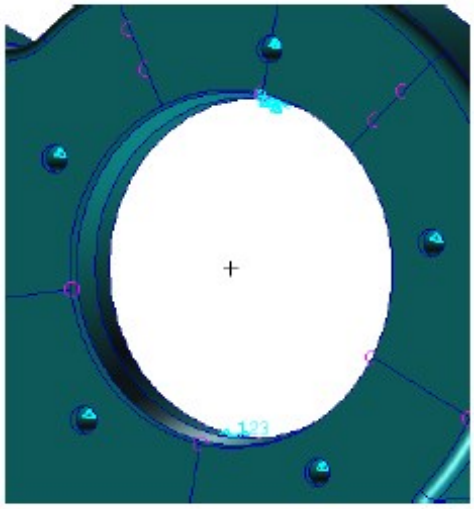

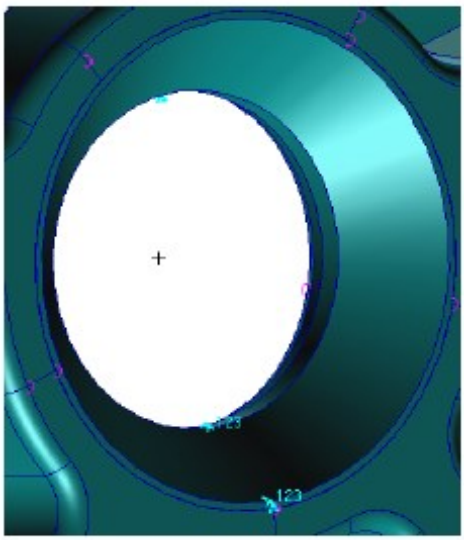

Radial Total Load

Lateral Total Load

Longitudinal Force

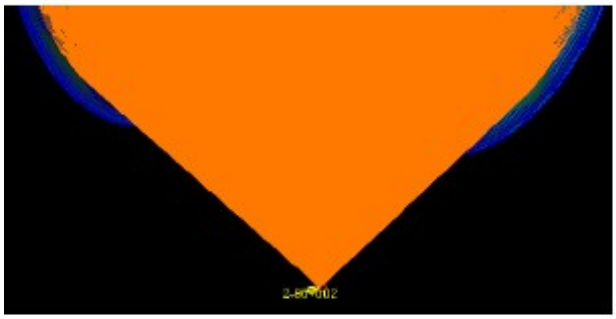

Pressure

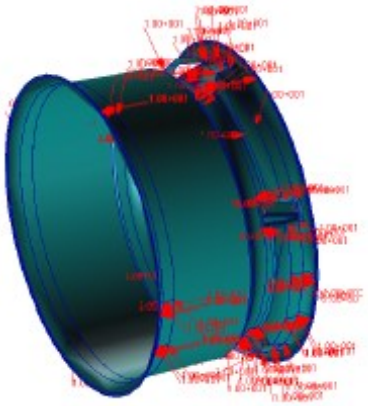

Result Plots:

Displacements (Magnitude)

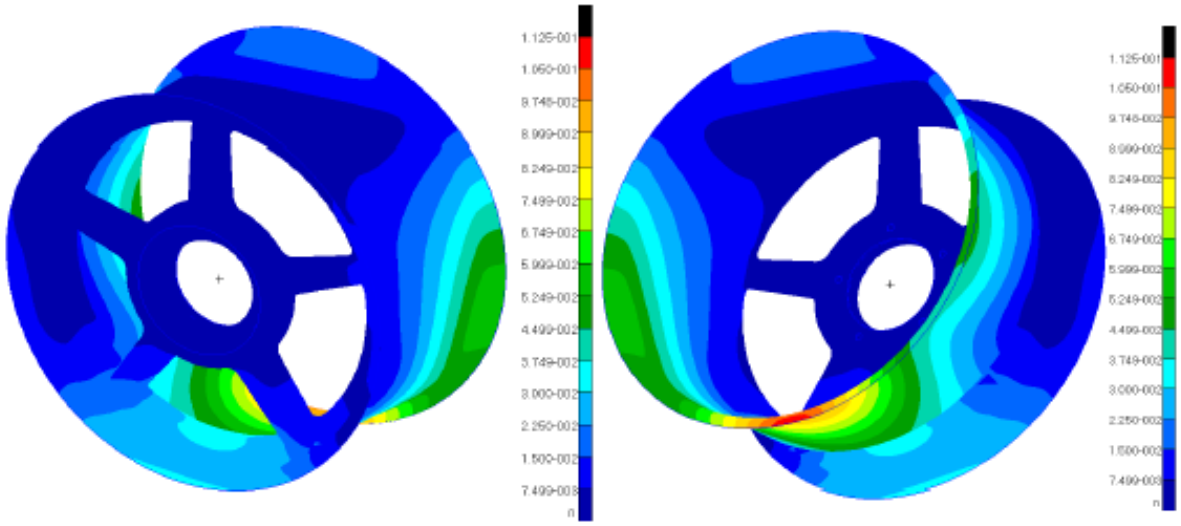

Hoffman Stress Worst Reserve Factors

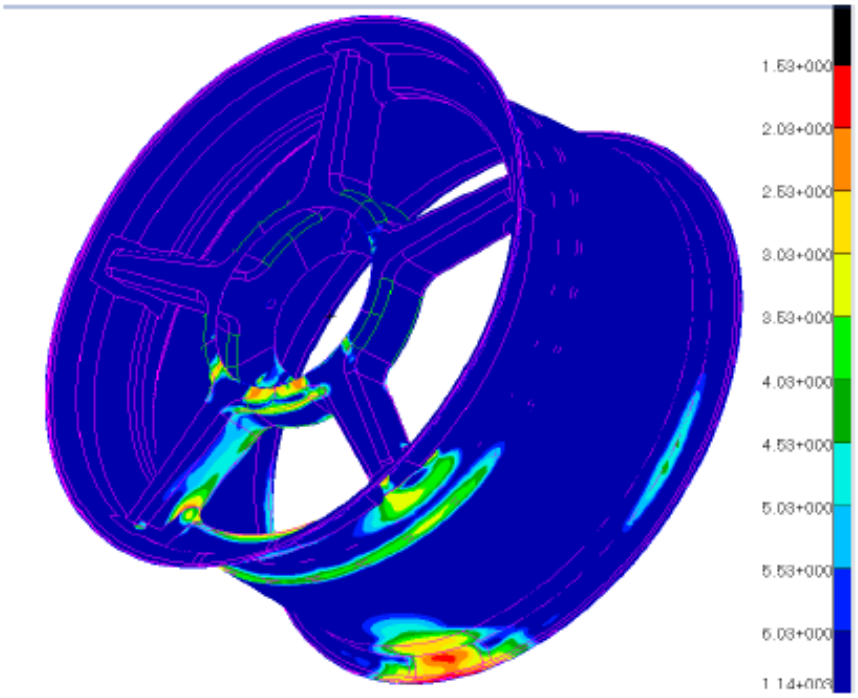

Tsai-Wu Stress Worst Reserve Factors

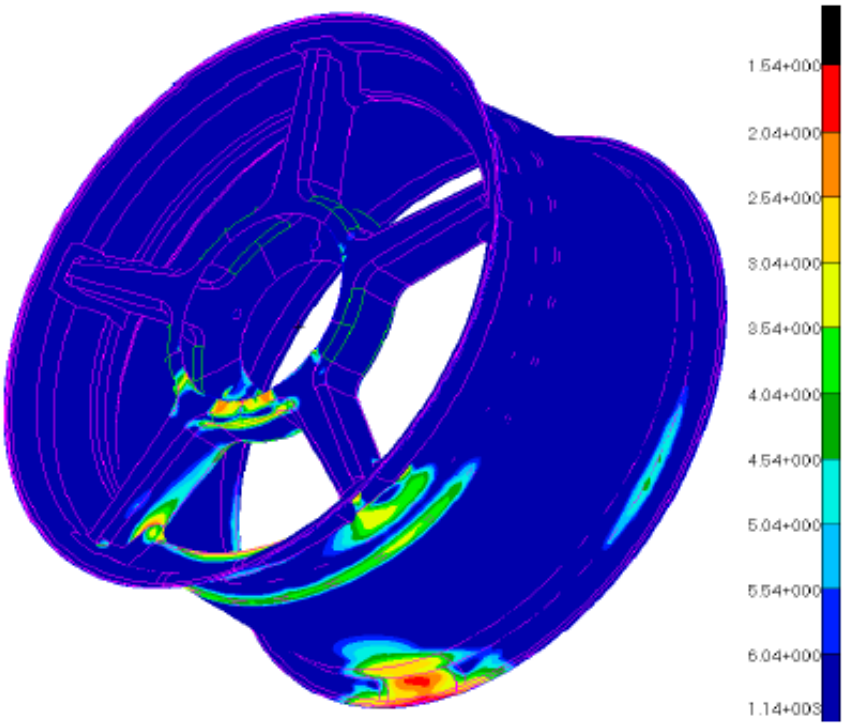

Maximum Stress Worst Reserve Factors